C/S NW 789223

FINAL REPORT

JUNE 1, 1984 THROUGH NOVEMBER 30, 1985

NASA GRANT NO. NSG 2291

COMPUTATIONS AND TURBULENT FLOW MODELING IN SUPPORT OF HELICOPTER ROTOR TECHNOLOGY

Prepared for:

Experimental Investigations Branch
NASA-Ames Research Center
Moffett Field, CA 94035

by:

William C. Rose
Engineering Research and Development Center
University of Nevada, Reno
Reno, NV 89557

FINAL REPORT

JUNE 1, 1984 THROUGH NOVEMBER 30, 1985

I. BACKGROUND

This report serves as the final report for the present Grant. Since many topics of study have been undertaken over the lifetime of the Grant and each of these topics has been documented in a sequence of progress reports submitted under the Grant, this final report will contain only discussions relating to the final effort conducted during the Grant. In the present reporting period, emphasis was focused on the behavior of turbulent flow and its modeling and scaling over and within open cavities. In particular, how the turbulence effects optical transmission through such turbulent flowfields was of interest.

During the course of the Grant it has been noted that one of the least well understood aspects of turbulence is scaling between wind tunnel conditions and those of flight. Of particular interest in the current phase of the Grant is the degradation of the optical performance of an airborne telescope and how proposed and recently completed wind tunnel experiments can be used to shed light on the actual airborne performance of such an optical system. The Kuiper Airborne Observatory (KAO) operated by the NASA-Ames Research Center is an example of such a flying full scale airborne optical system.

Two major issues can influence the overall performance of such airborne optical systems. The first is the mechanical environment in which the optical system must perform. This environment includes the vibration input to the optical system through the aircraft motions and that due to an

unsteady pressure environment that may exist surrounding elements of the optics. Depending on the scale size and magnitude of the pressure variations, loads on the optics may produce deflections that can cause degradations of the performance of optical elements placed within an open cavity. Effects that unsteady airloads have on optical performance have been successfully minimized in the past. Devices such as porous fences mounted upstream of the open cavity serve to eliminate aero-acoustical resonances and reduce the random pressure fluctuation level within the cavity. Other techniques for improving the aero-mechanical performance of open cavities have been proposed. One such technique involving the use of active flow control and an aerodynamically contoured rear lip has been the subject of a recent wind tunnel investigation carried out in the 14 foot wind tunnel at the NASA-Ames Research Center. Once the pressure fluctuation environment has been made acceptable, the performance of optical systems located within the environment remains an open question. It has been shown that turbulence can degrade the performance of both projection and receiving optical systems. It is known that aerodynamic flowfields containing turbulence have an adverse affect on optical systems through the production of index-of-refraction fluctuations that can be seen by the optical system. It is this latter subject of aero-optics that is of interest during the current portion of the Grant.

Two independent studies have been conducted recently that examine the performance of optical systems subject to various forms of unsteady aerodynamic motion. One is the full scale airborne experiment conducted on the NASA-Ames Kuiper Airborne Observatory in two phases; the first of which was conducted under a program known as the "Seeing Study" and the other another portion of that program conducted under the "KITE" Program

carried out during the summer of 1985. The other program is a wind tunnel test conducted during the spring of 1985. This test was chosen to simulate the essential elements of the Airborne Optical Adjunct (AOA) tandem cavity configuration. The forward cavity of the AOA wind tunnel test can be considered as a model of the single KAO open cavity configuration. The interrelationship between studies ongoing on the KAO and the results obtained in the AOA wind tunnel test are discussed in this report. The interrelationship and the data obtained from these two experiments can shed light on the scaling of wind tunnel data to the full scale flight environment for such open cavity configurations.

In addition to the above, data were obtained on the KAO in a previous investigation and indicated substantial temperature variations occur with time in the KAO cavity. During the period of the present study, mean temperature data were obtained that allow the nature and sources of temperature differences existing within the cavity to be determined. These data will be discussed here in light of their application to reducing the optical degradation on the KAO as well as their impact on potential AOA programs.

II. INTRODUCTION

In the present reporting period effort was devoted to several specific tasks. These tasks are briefly outlined here and are discussed in detail in Section III. The first task was the preparation for the AOA tandem cavity wind tunnel experiment. Effort on this task was carried out between 1 June 1984 and the beginning of the actual wind tunnel test phase starting shortly after the beginning of 1985. The second task was the design and support of installation of a multi-probe aerodynamic rake for use in surveying the shear layers present over the open cavity on the KAO. The third task consists of supporting several KAO flights throughout the reporting period in order to determine the nature of the behavior of the thermal environment within the KAO cavity at operational altitudes. This effort is an extension of effort previously conducted under another contract which was carried out during the Phase I "Seeing Study" flights. The fourth task was in the assistance in the design of the cavity for the University of Denver radiometer.

The beginning of the following section contains a discussion that attempts to distinguish between the optical terms of blur circle size (or image size) and the term due to jitter. The discussion attempts to show why aberrated focal plane images due to turbulent flow must be considered essentially a two-part analysis; one of which produces a jitter of the spot, while the other produces an increased spot diameter. Previous investigations on the KAO have tended to confuse these issues by not properly separating the effects of very large scale turbulence and those due to relatively small scale turbulence. For example, the observations quoted in the "Erickson Workshop" of October 1982 indicate that image size decreases substantially

with decreasing exposure time. We now believe, according to the analysis presented in the first part of Section III, that this decrease is related to the jitter contained in the longer time exposures, while the asymptotic spot size is related to scale sizes that are typically much smaller than the diameter of the focusing beam at any point throughout its path.

III. DISCUSSION

III.1 THE INTERRELATIONSHIP BETWEEN OPTICAL PERFORMANCE AND TURBULENT FLOW

Although the interrelationship between fluid mechanics and the behavior of coherent radiation is of great importance to many operational as well as proposed electro-optical systems, the interrelationship is not well understood. Historically, focal plane image quality and atmospheric turbulence has been linked since early astronomical observations. More recently, interest in turbulence effects on optical systems has spread to many other areas. The basis of the interrelationship can be considered with the aid of the following discussion.

Consider a series of uniform sized phase distortions present in a gas into which an initially plane wavefront is propagated. As long as the diameter of the optics is substantially less than the size of the phase disturbances, the wavefront emerges with a time-dependent tilt. The so called "image dancing" analyses such as that proposed by Huffnagle describe this case. The motion of the spot is given by the difference in phase between the two edges of the aperture divided by the diameter of the aperture. However, this simplified analysis becomes much less trivial (even in concept) when multiplicity of phase distortions of various sizes are present in the fluid.

For cases in which scale sizes become less than that of the optics diameter, the effect is no longer simply one of focal plane motion. As the optical scale size becomes smaller and smaller, energy becomes scattered out of the initially defraction limited spot into ever increasing size circles in the focal plane. In the limit of extremely small size turbulence, the focal plane

peak intensity relative to its defraction limited value (also known as the Strehl Ratio) decreases. With increasing strength of the turbulence more and more energy is scattered until, finally, little detectable energy remains in the central lobe (defraction limited area).

The above two cases represent limiting conditions for the optical performance of any practical optical system operating in the presence of fluid mechanically induced phase distortions. In reality, all fluid mechanical turbulence possesses some continuous spectrum of scale sizes. There can exist both scales smaller and larger than any mathematically defined integral scale size. For scale sizes that are larger than approximately four times the diameter of the aperture only optical tilts will be produced. On the other hand, scale sizes smaller than approximately the aperture diameter divided by ten should be directly treatable from wide angle scattering analyses. For scale sizes between these two limiting cases, corresponding optical aberrations that may be expressed as Zerneke polonomials will be required to describe their optical effects. From results of the Air Force program in high energy laser propagation, it is believed that large low order errors (such as focus) can arise from scale sizes whose motions correspond to sizes between about four times the diameter and two times the diameter of the optics. Scales between approximately twice and half the aperture diameter produce higher order errors (e.g., astigmatisms and comma). In a very simplified form, one might assume that the spectrum may be broken into two scale sizes, one of which characterizes the large scale motions and the other which characterizes the small scale motions. One might also assume that this division occurs when the scale size to diameter ratio is near one. An integral scale size may be defined from the spectrum of the motions on either side of that dividing size and the relative weights of the

phase variance may be applied in each of those bands. The large scale sizes can be thought of as producing wavelength independent focal plane jitter. The small scale data can be thought to produce a near instantaneous blurred focal plane image. This instantaneous blurred image will also be subjected to the long time jitter (beam wander) term from the low frequency side of the spectrum.

III.2 Preparation for the AOA Wind Tunnel Experiment

Effort was expended under the present Grant in order to ensure proper planning and preparation for the AOA Tandem Cavity Wind Tunnel experiment. Several technical interchange meetings were attended in conjunction with personnel from JPL, NASA-Ames, TBE, and the U.S. Army MICOM. Initial planning and layout of the design of the model and its relationship to the expected platform design was of critical importance. However, because of the fact that the BMD prime contract for the AOA platform had not been let at the time of planning the wind tunnel test, only a generic wind tunnel model could be designed. Previous experience in generating appropriate upstream conditions for use in open cavity experiments in wind tunnels was used to select boundary layer thickening pins to achieve boundary layer heights at the forward cavity representative of those that could be envisioned from any of the AOA prime contract concepts. Thus, compatability between any selected platform contractor's concept and the AOA wind tunnel model could be insured.

Arrangements were made for use of NASA-Ames unsteady aerodynamic equipment including unsteady pressure instrumentation, as well as broadband amplifier instrumentation required for use in the actual conduct of the wind tunnel test. Additional arrangements were made with the U.S. Air Force Weapons Laboratory for use of their entire hot-wire anemometry package including both constant temperature and constant current bridges for measuring unsteady density in the cavity as well as in the shear layers occurring over the tops of the cavities. Pretest meetings held at NASA-Ames were attended and continuous input into the design phase of the wind tunnel model was offered to JPL. The model mockup meeting at JPL was attended.

During the course of the planning phase of the test, several design concepts for a movable probe drive were investigated. The ultimate selection was for the JPL probe drive because of its ability to be changed to viewing angles other than 90 deg to the external flow. It appeared that the JPL probe drive, although potentially fraught with other problems, would be the only conceptually useful drive system.

Because of findings concerning the variation of temperature from point to point and as a function time within the KAO cavity at operational altitudes, the requirement to include a heater system in the forward cavity of the AOA wind tunnel model was generated. Simulation of this temperature variation was to provide a temperature differential between the cavity gas temperature and that of the solid surfaces of the cavity. This heating system was chosen to be generic in nature, and did not necessarily simulate either the AOA internal heat sources or those suspected of being heat sources on the KAO. A maximum of 1.6 kw could be put into the cavity.

This planning effort led, in part, to the successful accomplishment of the AOA wind tunnel test. The interrelationship between this test and those on the KAO are discussed later.

III.3 Airborne Aerodynamic Rake Design

During the time of the AOA wind tunnel test, it became evident there was a strong requirement to validate any potential scaling relationships that would be derived during the wind tunnel test or the post test data analysis. Of particular interest was the behavior of the turbulence in the shear layer over the open cavities. An ideal opportunity to verify the scaling relationships between wind tunnel and flight conditions for shear layers over open cavities became evident when considering the KAO as an airborne test bed. Initial conceptual studies indicated that turbulence data could be obtained on the KAO for various settings of the porous fence located ahead of the cavity. A scheme was devised that would allow measurement of the shear layer properties that would be comparable to those being measured in the AOA wind tunnel test on a non-interferring basis with ongoing astronomy flights. This involved designing a rake to be attached to the fuselage just downstream of the open cavity. The actual measurement station, that is the location of the sensors and tips of pressure probes, was to be located at the aft edge of the cavity.

Because of the potential large cost of such a probe and rake assembly, design considerations included the possibility of using the rake on any now flying aircraft. Thus, loads were assumed to apply on the rake for conditions beyond those normally encountered on the KAO. The rake was designed to be able to measure both the fuselage boundary layer, that is the relatively thin boundary layer when the fence is down and the door is closed (in order to relate airborne information to those obtained in the wind tunnel), as well as to be able to measure the shear layer properties with the door open and the fence deflected upward in the range of 30 deg to 90 deg. This requirement dictated a non-constant spacing of the sensors

on the rake that was sufficient to encompass the expected extent of the shear layers when the fence was deflected at the full 90 deg position. This yielded a rake 24 in long and probe spacings of a maximum of 1 in apart. This rake has 37 sensor sites. In addition to measurement of pitot pressure it was also desirable to make measurements of turbulence properties in the shear layer using similar hot-film instrumentation to that in the AOA wind tunnel test. The design was chosen so that pitot tube instrumentation and hot-film holding instrumentation could be interchanged with a minimum of effort. Thus, the single fixed rake system could be used on different flights to determine both mean and fluctuating flow parameters within the shear layers.

The rake was designed in conjunction with personnel from Northop Services Company. Input loads and expected unsteady variations to occur were given to Northrop personnel and were based on previous experience gained during the U.S. Air Force's Airborne Laser Laboratory (ALL) program. The unsteady loads assumed to occur on the KAO were taken as the maximum loads associated with the unsteady flowfields concerning the ALL turret turbulence values. This produced design values that were very conservative from the KAO viewpoint and led to a rather stiff structure and associated strong attachment points. The design was reviewed and approved by Stress Technologies, Inc. from Bellview, Washington. The rake was fabricated by MicroCraft and delivered to NASA-Ames in the fall of 1985. Figure 1 shows closeup photographs of the rake installed on the KAO in both the pitot pressure and hot-film anemometer configurations. Figure 2 is a rake installation photograph showing its position with respect to the telescope door and portion of the KAO fuselage.

III.4 Interrelationship Between the AOA Wind Tunnel Test and the KAO Flight Experiments

Although the forward AOA wind tunnel and KAO cavities are similar, slight differences exist. These are indicated schematically in Figure 3 where the AOA cavity is indicated on the left side of the figure while the KAO is on the right side. The cavity opening length in the streamwise direction in the wind tunnel test is 13 in and data were obtained at the mid position of the cavity, that is $6\frac{1}{2}$ in downstream of the forward cavity lip. The top of the fence is located approximately $8\frac{1}{2}$ in upstream of the instrumentation station for a representative 2 in-long fence at the 30 deg position. For the KAO, the cavity opening length is 56 in. The rake is attached as noted previously at the downstream edge of the cavity opening thus giving a distance of approximately 64 in from the top of the fence to the instrumentation station. The KAO fence is approximately 7.8 in long and about 40 percent porosity. It can be positioned continuously from 30 deg to 90 deg in flight. A representative 30 deg setting gives approximately a 64 in distance from the top of the fence to the instrumentation station. Figure 4 summarizes the important parameters effecting the scaling of wind tunnel and flight data and the comparison of those parameters for the AOA and KAO.

Two very important parameters are the upstream boundary thickness, δ_o, and the streamwise length of the cavity opening, x_c. For the wind tunnel test, the streamwise opening was 13 in and the boundary thickness chosen was 1 in. These same numbers for the KAO are 54 in and 4.2 in, respectively. The ratio between the wind tunnel and KAO for both of these critical parameters is a value near 4.2. The ratio of the fence length chosen to be the most effective in the AOA wind tunnel test to that

of the KAO is near 3.9, while fence angles and porosity are nearly duplicated. Another important parameter of Mach number was chosen in the wind tunnel test to be .5, .62, .7 and .8 while the KAO typically operates between approximately M=0.7 and 0.8. As can be seen, excellent scaling between the forward cavity in the AOA wind tunnel test and the KAO exists. Thus, data obtained using the rake system on the KAO should lead to meaningful scaling law validation.

III.5 University of Denver Radiometer Cavity Design

During the course of the present Grant, design inputs were given to NASA personnel to aid in cavity resonance elimination for the proposed University of Denver radiometer site located forward of the front crew access door on the KAO. Using experience gained in the recently completed AOA tandem cavity wind tunnel experiment, it was found that nearly all cavity resonance could be eliminated with an efficient aerodynamic rear lip. Although originally proposed by Boeing to be used in conjunction with active flow control concepts, the rear lips themselves eliminated nearly all of the cavity resonance problem. The proposed radiometer opening in the streamwise direction only spans a distance of approximately 4 in. With the turbulent boundary layer thickness at the radiometer station estimated to be at least 2 in, the prospects of having an uncontrolled cavity oscillation are small. The addition of a smooth aerodynamic rear lip was designed to ensure not only elimination of cavity resonance but also to produce small random pressure fluctuations within the cavity. The recommended rear ramp was simply a scaled down version of the modified Boeing Aerospace Company (BAC) ramp denoted in the AOA wind tunnel test as "12-45-L." The ramp was scaled such that it overhung into the cavity about 1.5 in. Since this contour is a two-dimensional contour and the radiometer opening is a slit in the surface, the ramp contours were faired around the upper and lower edges of the slit.

The airworthiness flight of the KAO following extensive cavity modifications was also an evaluation flight for the University of Denver radiometer cavity. The radiometer was not in place during this flight so that the effectiveness of the cavity design including the aft ramp could be evaluated. It was found that no perceptible resonance or broadband

pressure fluctuation sound levels could be detected within the cockpit at operational altitudes. Thus, the use of the AOA wind tunnel validated rear ramp configuration was successfully applied to a full scale opening in the operational KAO.

III.6 KAO Cavity Thermal Behavior

Results from the "Seeing Study" conducted in June-July 1984 indicated the potential for large temperature variations to occur within the cavity gas from point to point and with time at a given point. Upgrades in cavity environmental monitoring capability occurred between the Seeing Study and the KITE array flights conducted on 5, 7, and 8 June 1985. This newly installed instrumentation could shed light on the steady-state temperature differences within the gas and also included six new mean temperature sensors attached to the backside of the primary mirror. The following discussion is based on analysis of this new instrumentation and data taken from it on the 1985 KITE array flights. Note that the high response thermal instrumentation used on the Seeing Study was not installed for these flights so that only steady-state data are available.

Upon preparation for the flight series it was discovered that four of the six wall sensor temperatures located in the cavity, although operational for previous flights, were assigned incorrect nomenclature in the ADAMS and TDADS programs.

Actual Sensor Site	Indicated TDADS Readout
BA	TF
LW	BA
TF	BF
BF	LW

These improperly wired four sensors must be borne in mind when viewing any cavity environment thermal data obtained prior to 6 June 1985. The wiring arrangements were corrected on 7 June 1985 and, in addition, ice point calibrations were applied to all sensors throughout the cavity. Some of the temperature sensor's offsets varied up to 5°C from those

nominally assumed in prior flights. These new calibrations were added to the automatic data system.

A specific change in the temperature sensor hardware arrangement was made for the current flight series. The two temperature sensors located on the surface of the insulation of the aft bulkhead were removed and replaced with probe-type air temperature sensors set on offsets so that true air temperature may be obtained rather than the surface temperature of the insulation in the cavity. This was done because of the unknown value of heat transfer that exists in flight through the insulated cavity bulkhead and walls. The following discussion presents the data from the three flights and a discussion of the observations.

All three flights from the KITE II sensor array studies were flown on local times of the 4th, 6th and 7th of June. The universal time dates are the 5th, 7th and 8th of June, respectively. In this discussion all times are referenced to the flight universal time.

The data from flight 1 are discussed with the aid of the mean temperature variations with time displayed in figure 5 for various sensors. During flight 1 several planned sequences during which the outside telescope door was to be closed were taken in an attempt to establish the equilabrium temperature of the components within the cavity. This is similar to the door closed sequences obtained in the Seeing Study conducted in June/July 1984. Six temperature sensors are installed on the back of the primary mirror in order to establish the backside surface temperature of the major thermally massive element within the cavity. These temperature sensors are arrayed in a radial pattern with temperature sensor T1 being at the outermost or largest radius, while sensor T6 is located near the center of the mirror. Figures 5a and 5b show the variation with time throughout

the flight of these backside mirror temperatures in comparison with a representative cavity air temperature sensor located at the aft top wall of the cavity. This sensor, AT, and a similar sensor, AM indicating aft mid temperature, are actually located on probes (even though the TDADS indicates a wall mount) that are positioned on standoffs so that they are more likely to sense actual air temperature in the cavity as opposed to being in contact with a wall surface. As we will see later, this distinction is probably irrelevant from an engineering view of the cavity environment. It is evident in figures 5a and 5b that a nearly exponential decrease of the backside mirror temperature with time is present and tends toward the cavity air temperature. The mirror temperatures started at the beginning of the flight at approximately -18 to -19°C indicating a good precool. It is noteworthy that temperature #4 in this sequence appears to be representative of those backside mirror temperatures and is used as the representative mirror temperature in future discussions. The exponential decay of the mirror temperature with time confirms the hypothesis set forth in the final report of the aerodynamic study conducted in the Seeing Study. However, a very bothersome feature of the data shown in figures 5a and 5b is that during door closed sequences, the air temperature quickly attains a value in excess of any of the backside mirror temperatures. Since the backside mirror temperatures are expected to be the warmest in the cavity, this behavior is somewhat puzzling.

In order to obtain additional information concerning this behavior, additional data were examined. For example, figures 5c and 5d compare the wall and cavity air temperatures with the perceived infrared (IR) air temperature given from the onboard water vapor emission sensor. As can be seen, cavity air temperatures as well as the cavity wall temperatures follow

the general trend of outside IR air temperature. The notable difference is the shift of the level due to aerodynamic heating due to the recovery temperature of the gas as discussed in detail in the Seeing Study final report. The air temperature at the top of the cavity is nearly the same as that of the left wall temperature and is also the same as the wall temperature located at the top of the forward bulkhead. In contrast, the mid-aft wall temperature appears to be consistently higher than those previously described. Furthermore, the right wall temperature, which is a sensor located near the bottom of the telescope cavity in back of the primary mirror, appears to also be consistently higher than all of the others discussed. Again, all sensors indicate substantial increases in perceived temperature during the door closed sequence. The fact that up to 5 to 6°C temperature differences are constantly present from the right to left walls of the cavity indicate either a strong conductive heat transfer path through the right side of the telescope cavity or the continuous leak of warm cabin air into the cavity. These temperatures are again seen in figure 5e to rise above the representative mirror temperature giving credence to the existence of a rather high response thermodynamic path into the cavity. This path is one not simply due to the conduction through the insulated cavity wall. Similar information is seen in figure 5f which also shows the spider temperature. This latter temperature is sensed with a wafer located on the outboard side of the spider and is set in epoxy which may not be in good thermal contact with the spider material, itself. The trend of the spider temperature being consistently lower than that of any other wall or gas temperature in the cavity persisted throughout this study. It is also clear from the data shown in figure 5f that the spider response time is much longer than that of any of either the air or other

wall temperature gages. This is probably due to its imbedding within the epoxy mass. One potential cause of the spider temperature to read low is that it is radiatively coupled to the night sky at altitude.

Just after flight 1, a conserted analysis of the foregoing data was undertaken. Based on the data shown in figure 5, it was concluded that there are cabin to cavity air leaks. It can also be concluded that the door closed data in the presence of such unknown air leaks are not representative of the cavity equilibrium temperature. Just prior to the mission briefing for flight 2, figure 5g was generated from flight 1 which shows the circulation duct temperature as compared with representative data shown previously. From these data, it is obvious that the temperature at the bottom of the circulation duct is much higher than any other temperature located throughout the cavity (in spite of the fact that this circulation duct temperature at the beginning of the flight was approximately the same as the backside of the mirror temperature). Unexplained variations in the circulation duct temperature occur throughout the flight. On flight 2 much more attention was paid to the circulation duct temperature, since it was suspected that this may lead to the source of the major air leak into the cavity.

Figures 6a through 6h indicate data for flight 2 that are analagous with the data presented for flight 1 and are in the same sequence. In figures 6a and 6b, we first note that the effectiveness of the precool for flight 2 was not nearly as good as that of flight 1. A representative mirror temperature of approximately 6° to 7°C is seen at the beginning of the flight. Also evident from the mirror temperatures is the same previously noted nearly exponential change of temperature with time. Sensor T1 is near the outer edge and tends to follow more closely the air temperatures

within the cavity. Clearly evident also in figures 6a and 6b is a large increase in air temperature beginning at approximately 0630 and continuing to approximately 0900. The reason for this is clearly shown in figures 6c through 6d which indicate the outside IR air temperature also increased in this time period. The cavity air temperatures and wall temperatures follow closely this change in outside temperature. Door-closed sequences were also taken during flight 2 and indicate sudden increases in temperature as a result of the door closing similar to those seen in flight 1. It is interesting to note in figures 6e and 6f, for example, that at times during the warm outside air episode just discussed, that the cavity air temperatures are seen to come within 5° to 6°C of the representative mirror temperature, while at other itmes throughout the flight the difference between the air temperature and representative mirror temperature ranged up to approximately 20°C.

Because the circulation duct temperature appeared to be indicative of some sort of air leak occurring based on the data of flight 1, this temperature was monitored closely throughout flight 2 and is shown in comparison with representative wall and air temperatures in figures 6g and 6h. It is interesting to note that upon the first door opening sequence at approximately 0500 the circulation duct temperature begins to fall dramatically in parallel with the other wall and air temperatures within the cavity. However, that fall is interrupted and a return to a value of near -5°C is evidenced throughout the flight with the exception of a small episode near 0530 during which the duct circulation fan was manually activated and indicated a rapid decrease in the duct temperature. When the circulation fan was turned to the off position approximately 5 minutes later, the circulation duct temperature sensor immediately returned to a value of approximately -6°C.

Based on the data obtained from flights 1 and 2, and the strong indication of a major cabin-to-cavity air leak, during flight 3 it was decided to attempt inflight detection of the source of air leaks into the cavity. Several techniques were suggested for doing this; however, one technique was decided upon as being acceptable for inflight leak detection. This technique was the use of an ultrasonic acoustic sensor with a small hand positionable microphone. The principle of this instrument is the detection of frequencies in the bandwidth of approximately 20 to 40 kHz representative of those in air leak situations.

Data from flight 3 are shown in figure 7 for similar data as shown in figures 5 and 6. Figures 7a and 7b indicate the clear exponential decrease of mirror temperature from an initial value of approximately -8°C (and still decreasing at the end of the flight). The initial -8°C is again indicative that flight 3's effectiveness of precooling was not as good as flight 1. The circulation duct temperature as shown in figures 7g and 7h was closely monitored again. Upon door opening, in contrast to that observed in flight 2, the duct temperature did not fall. Possibly indicating that the aircraft was already at such a high altitude the pressure differences between the inside cabin pressure and that of the outside cavity pressure was such that substantial leaks were already occurring. Shortly after the beginning of the array measurement sequence, it was indicated that substantial frosting of the optical surfaces within the cavity had occurred. It is presumed that this frosting resulted from air leaks (yet to be detected from the cabin to the cavity). It is also interesting to note from the circulation duct temperature data that very erratic behavior between approximately 0500 and 0630 occurred. This behavior appears now to be linked to the change in elevation of the telescope and the positioning

of the open door near the top of the circulation duct. In this configuration, scavenging of the circulation duct is much more likely to occur and an inflow of cooler air from the cavity into the bottom of the duct is sensed when the telescope is at the higher angle. This hypothesis may also explain previously observed erratic behavior noted in flight 2. No further door closed sequences were attempted in flight 3 due to the potential admission of warm moist air from the cabin.

During flight 3, the ultrasonic leak detector was employed by first setting the gain to detect leaks in the escape hatches in the rear of the aircraft. With this gain setting the leak detector was taken to the right bulkhead access panel where leaks were immediately found that produced ultrasonic signals much stronger than those observed at the escape hatches. Further examination of the right bulkhead access panel indicated that leaks occurred at nearly every penetration into the cavity wall into which a bolt was placed to hold the door in position. After this detection sequence the ultrasonic sensor was taken to the forward bulkhead in and around the area of the circulation duct. A major leak in the circulation duct near the circulation fan housing was detected immediately. Air could be felt rushing past ones hand when placed near the position of the detected leak.

Further probing with the ultrasonic detector indicated that on the aft bulkhead, even the new feedthrough and closeout plate installation was a source of large ultrasonic signals, indicating potentially large leaks at this position. The cavity access door on the aft bulkhead did not appear to be a source of leaks even at the highest operating altitude. In summary, there were found to be leaks at almost every cavity penetration. A major leak was found in the circulation duct and was consistent with the observed circulation duct temperature data.

In flight 2, after discussion of potential leaks into the cavity, the principle investigating team sealed all of the bolt penetration holes into the cavity from the telescope backplate. On flight 3 this appeared to substantially reduce the difference between the aft-mid sensor temperature and that of the aft-top sensor temperature. The fact that plugging what appear to be minor leaks in any part of the cavity may strongly influence the perceived temperature at a specific site in the cavity indicates a need for ensuring the complete integrity of the seal between the cabin and the telescope cavity for future applications.

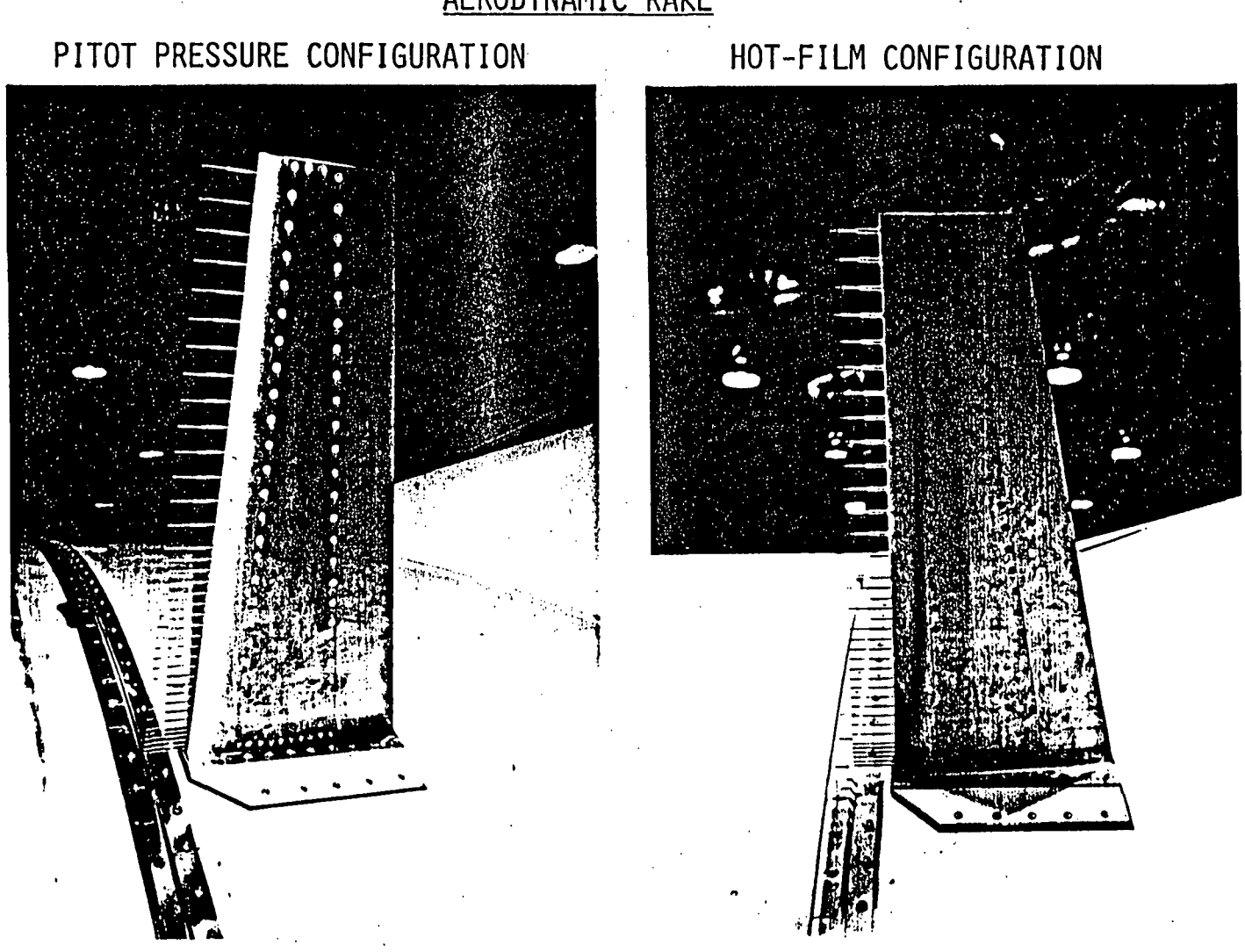

Figure 1. Aerodynamic rake shown in both configurations.

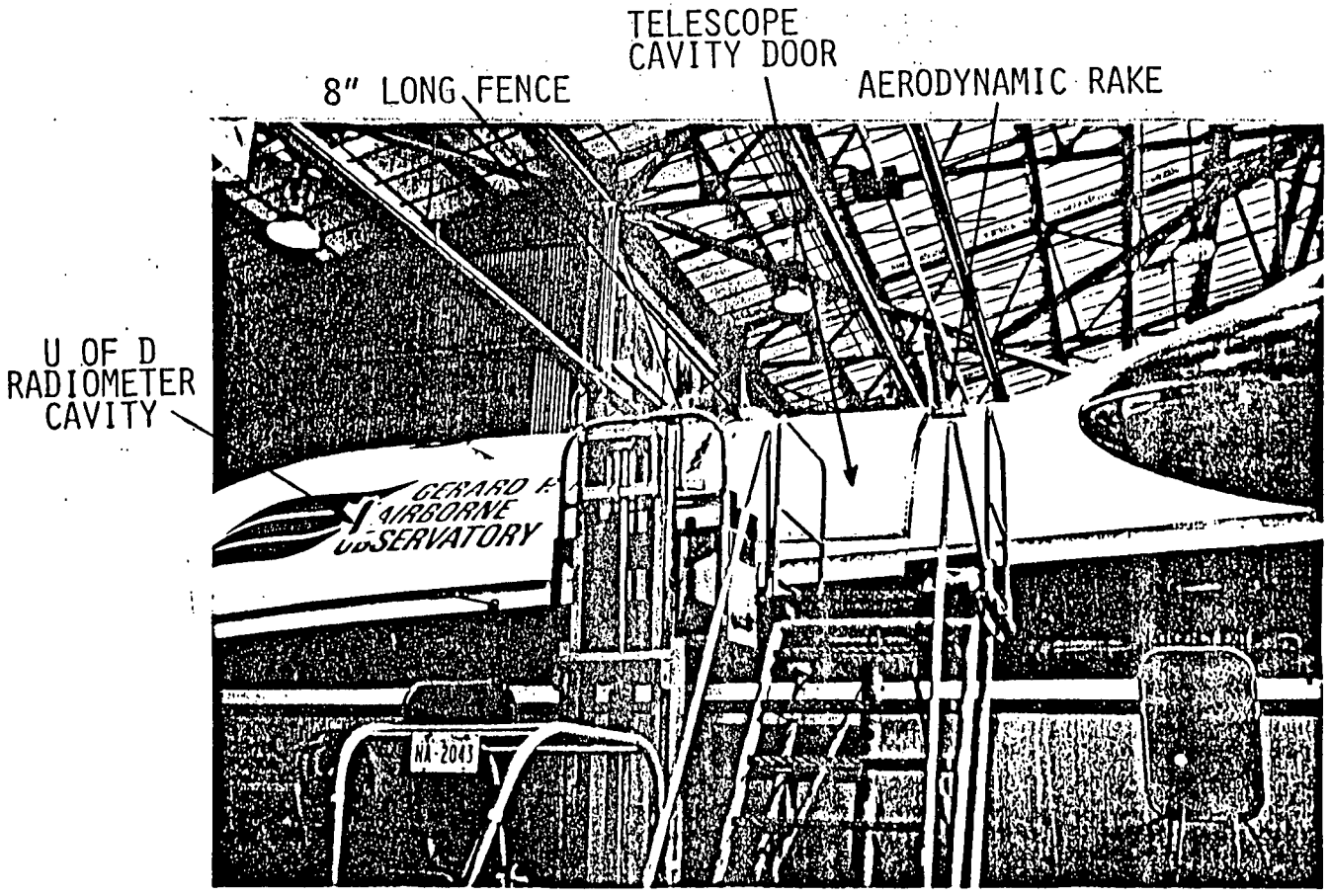

Figure 2. Installation of rake downstream of telescope cavity door.

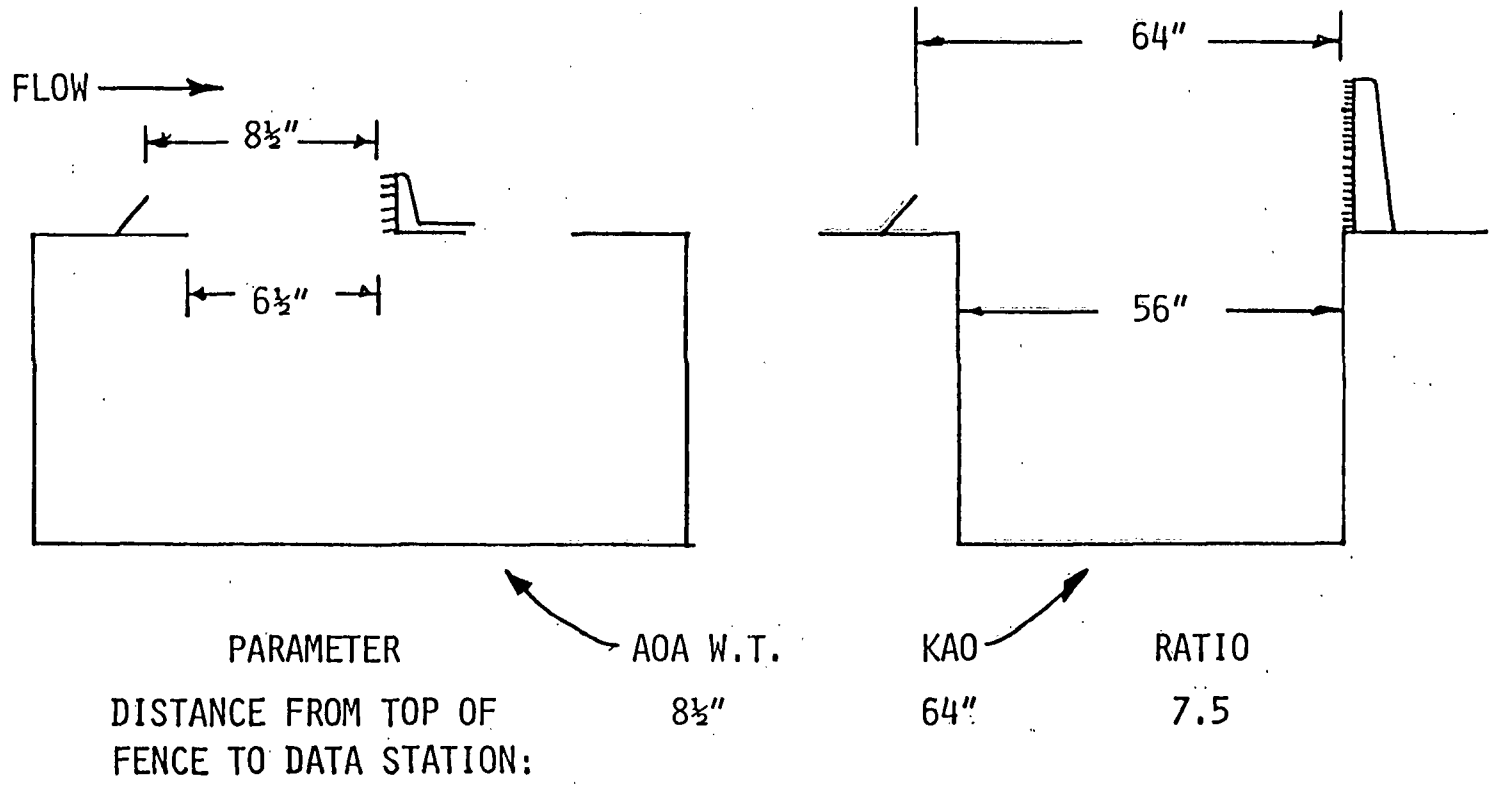

Figure 3. Schematic of AOA wind tunnel model and KAO cavities.

SCALING AOA W.T. AND KAO

- IMPORTANT PARAMETERS
  - δ_0; BOUNDARY LAYER THICKNESS JUST AHEAD OF DOOR
  - X_c; LENGTH OF CAVITY OPENING IN STREAMWISE DIRECTION
  - FENCE LENGTH
  - FENCE ANGLE
  - FENCE POROSITY
  - MACH NUMBER

PARAMETER	AOA W.T.	KAO	RATIO
δ_0	1"	4.2"	4.2
X_c	13"	54"	4.15
FENCE LENGTH	1",2",3"	7.8"	3.9
FENCE ANGLE	30,60,90°	$30 \leq \phi \leq 90°$	1.0
POROSITY	40%	$\approx$40%	1.0
MACH NUMBER	.5-.8	.7-.8	1.0

Figure 4. Important scaling parameters.

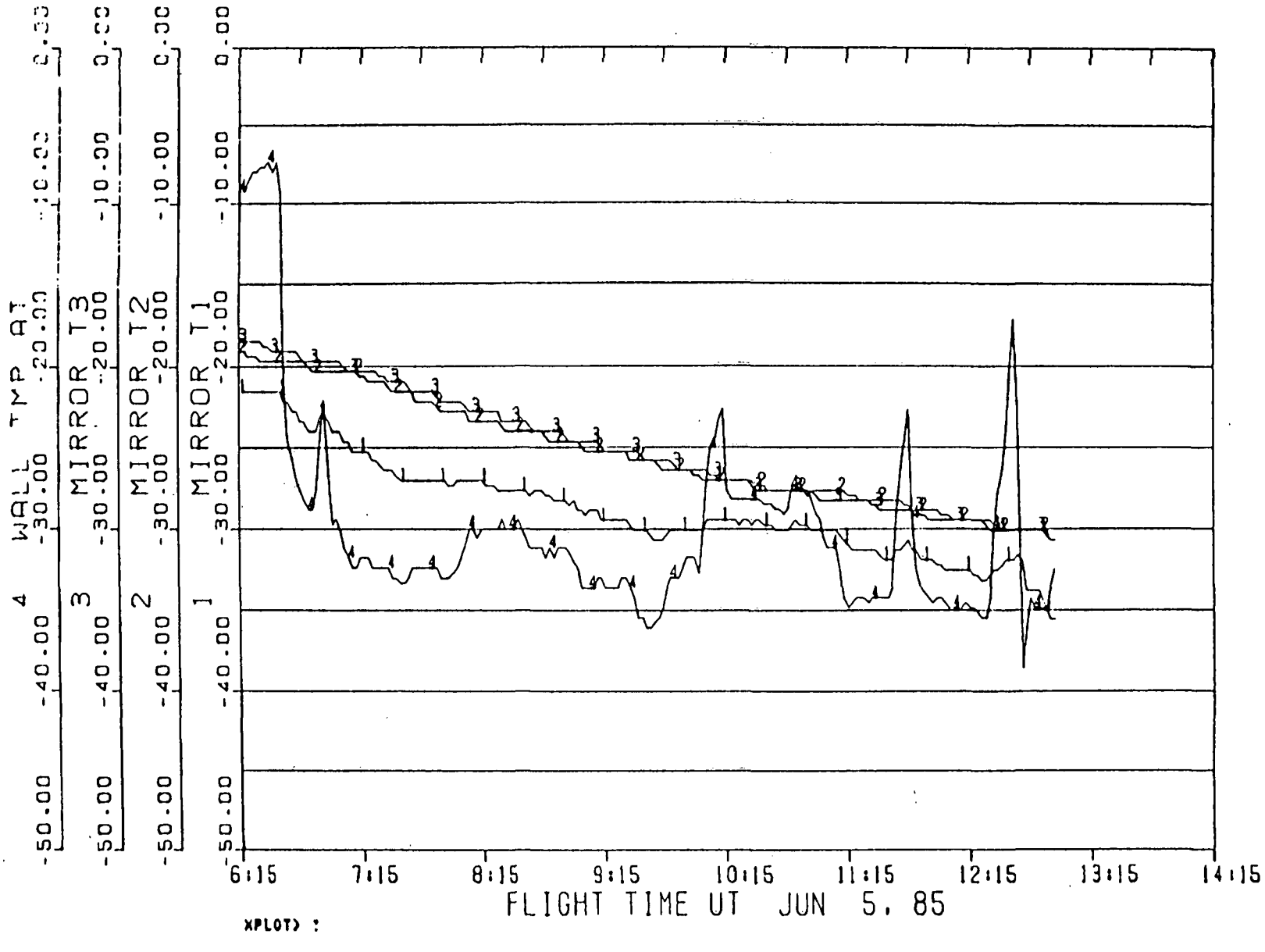

Figure 5. Mean temperature variation with time for KITE Array Flight 1.

a) Mirror temperatures 1, 2 and 3 compared with cavity air temperature.

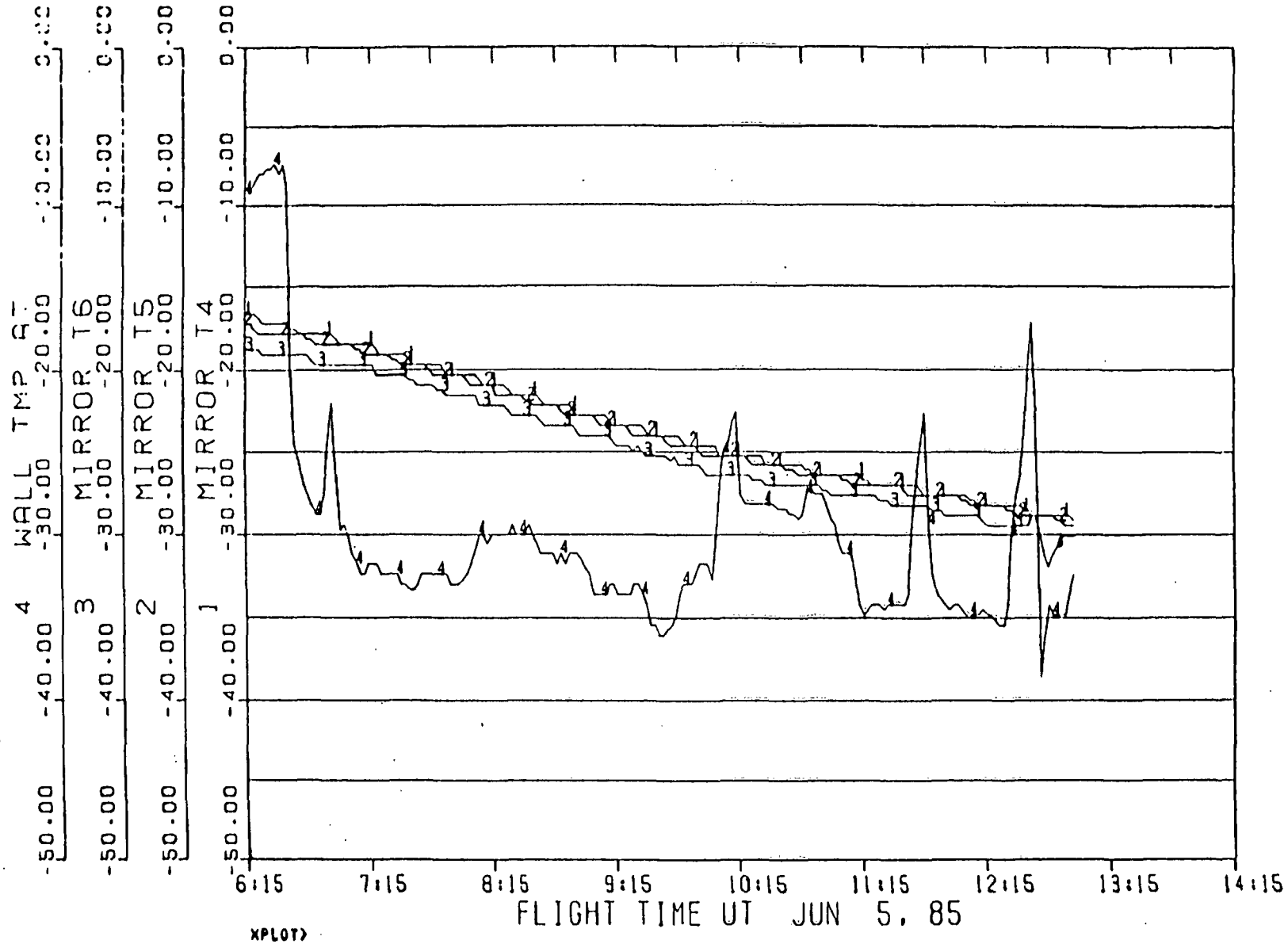

Figure 5. Continued

b) Mirror temperatures 4, 5 and 6 compared with cavity air temperature.

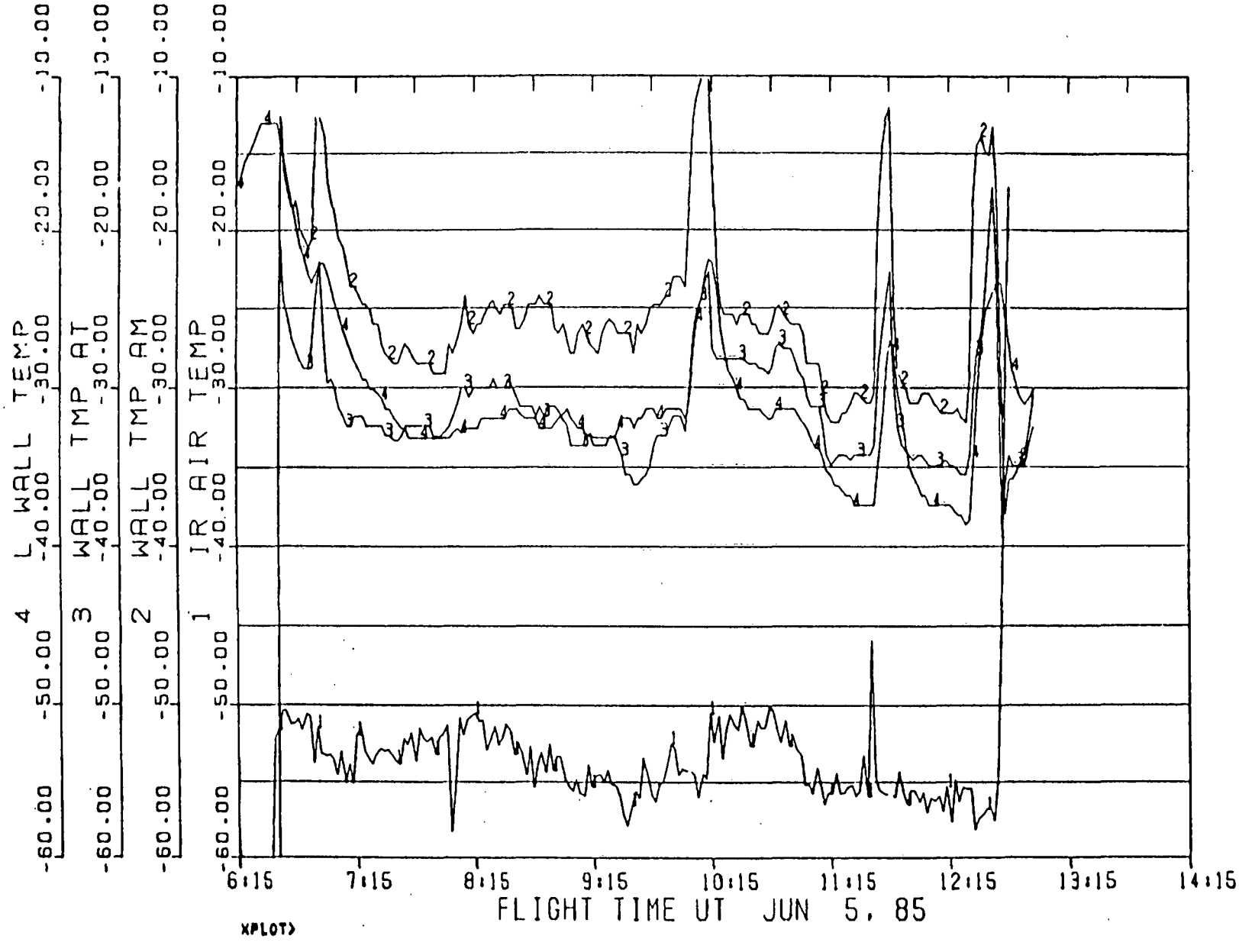

Figure 5. Continued

c) Left wall, IR air and cavity air temperatures.

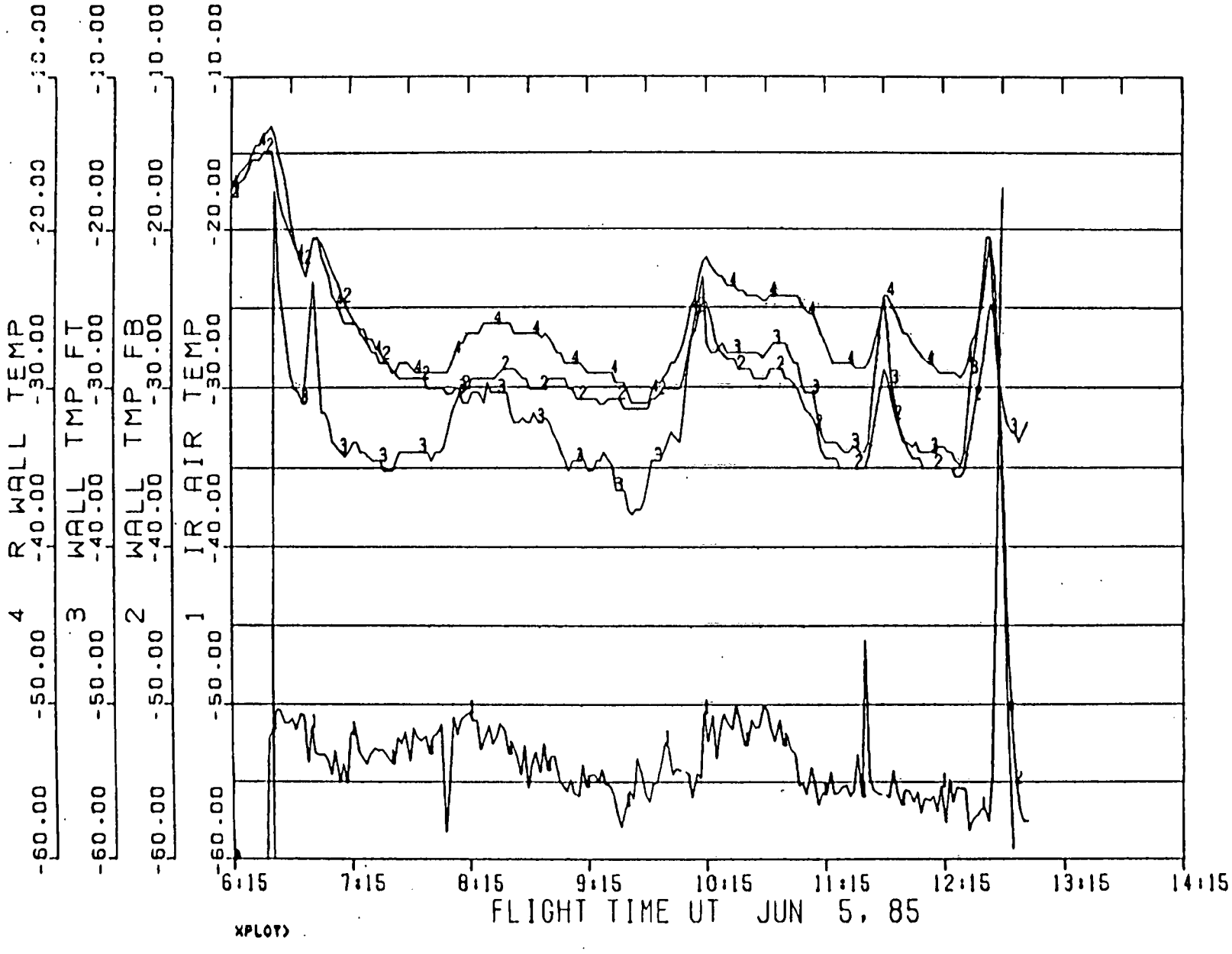

Figure 5. Continued

d) Right wall, IR air and cavity wall temperatures.

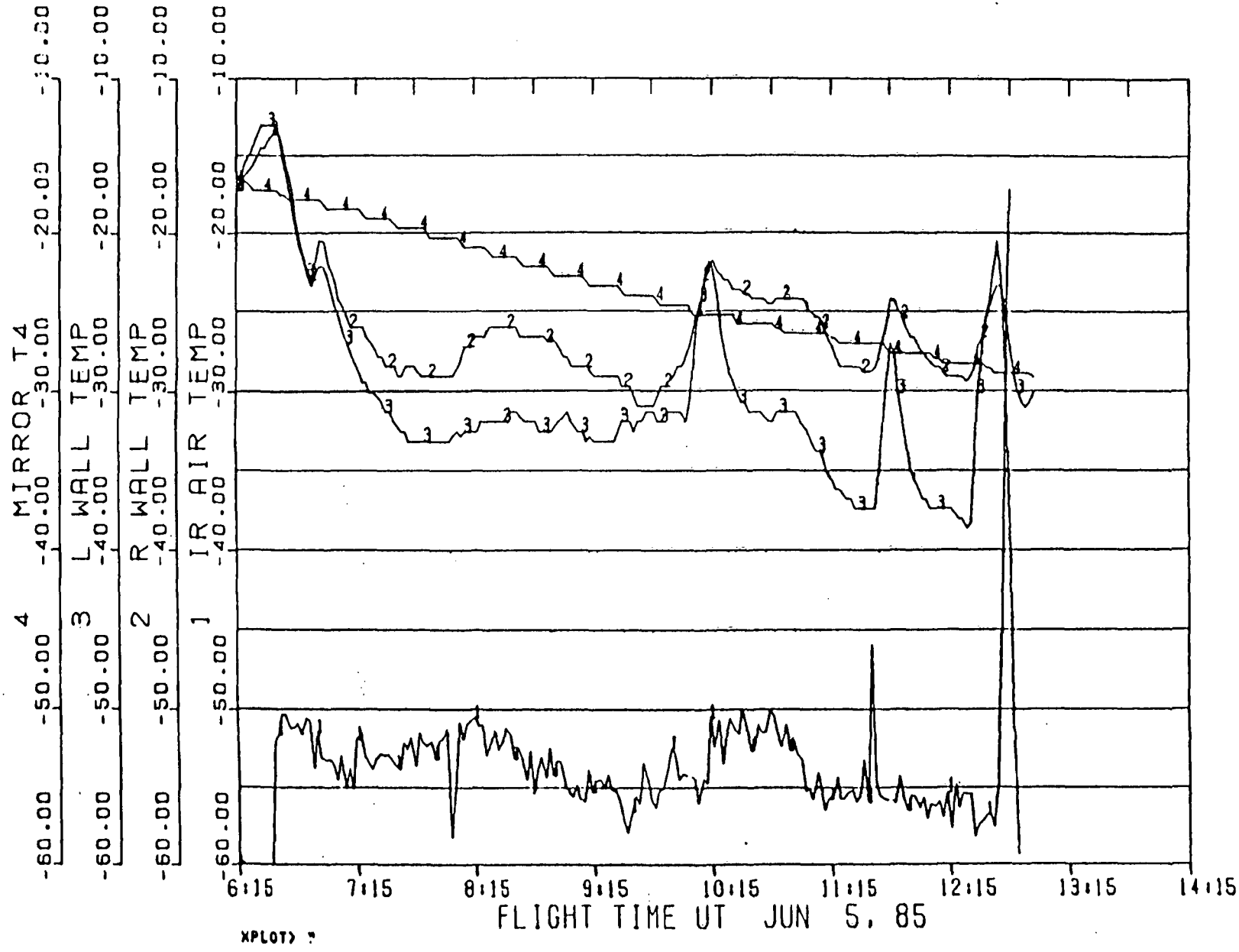

Figure 5. Continued

e) Representative mirror, wall, and IR air temperatures.

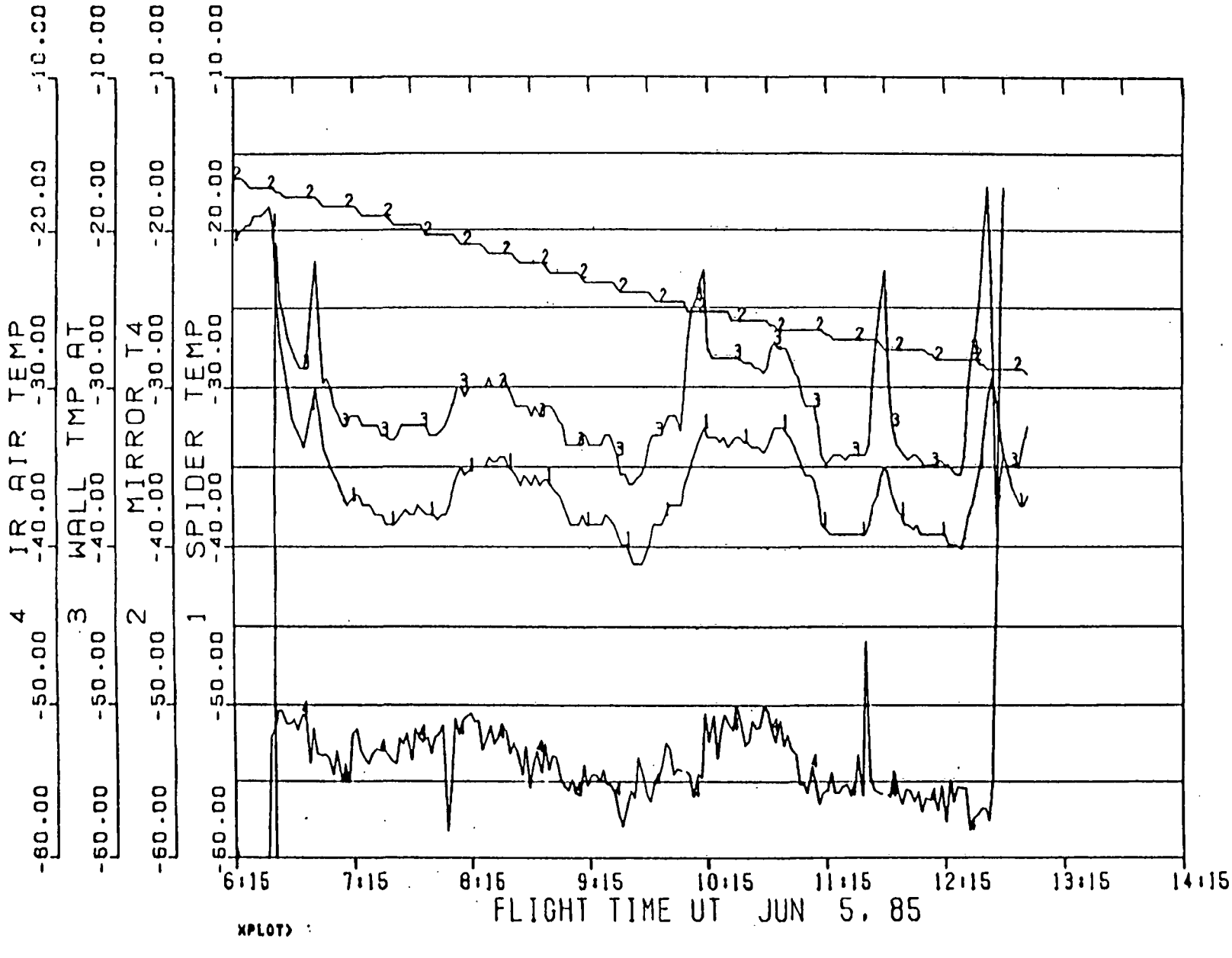

Figure 5. Continued

f) Representative mirror, cavity air, IR air and spider temperatures.

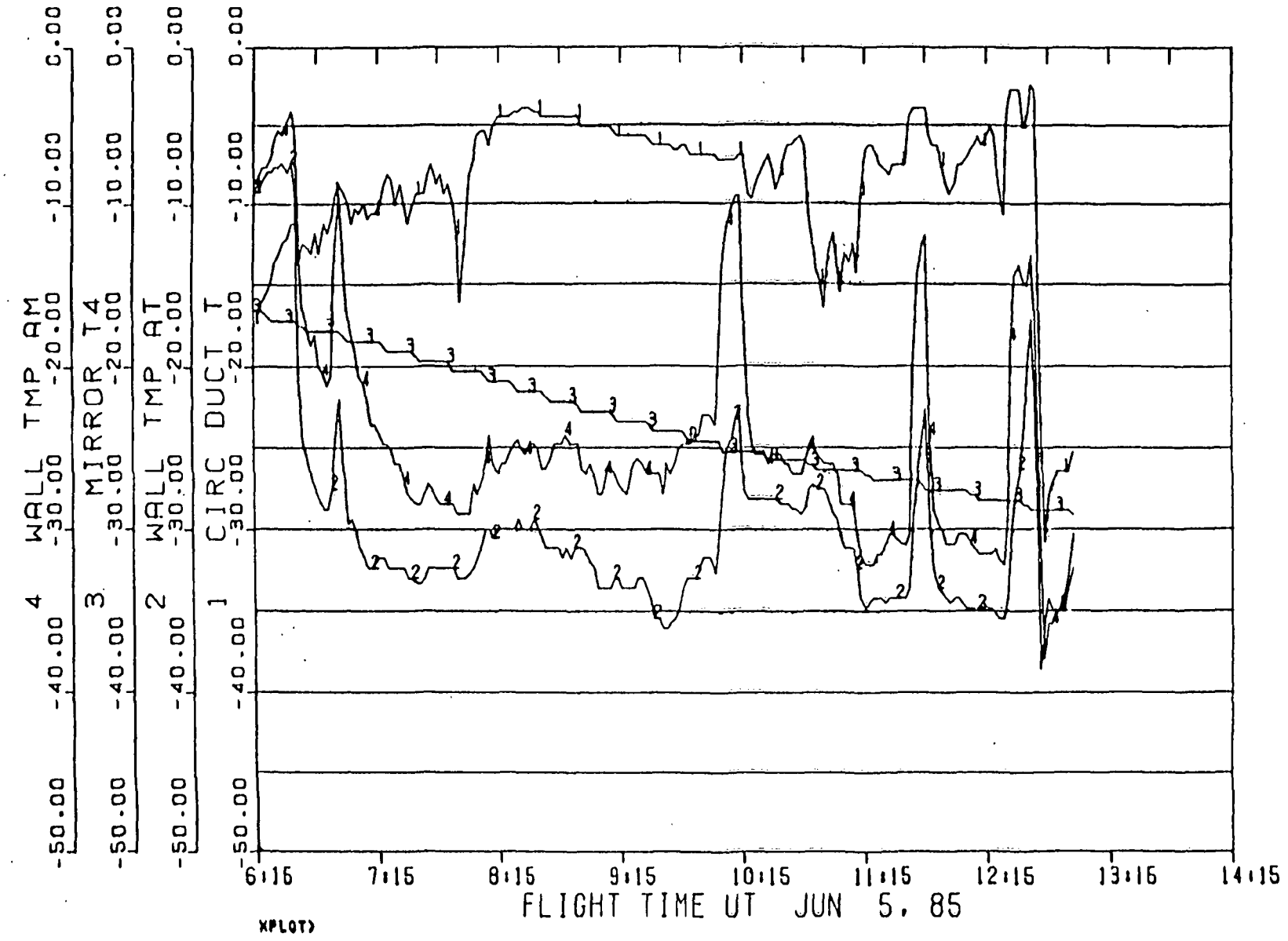

Figure 5. Concluded

g) Circulation duct temperatures compared with representative wall, mirror and cavity air temperatures.

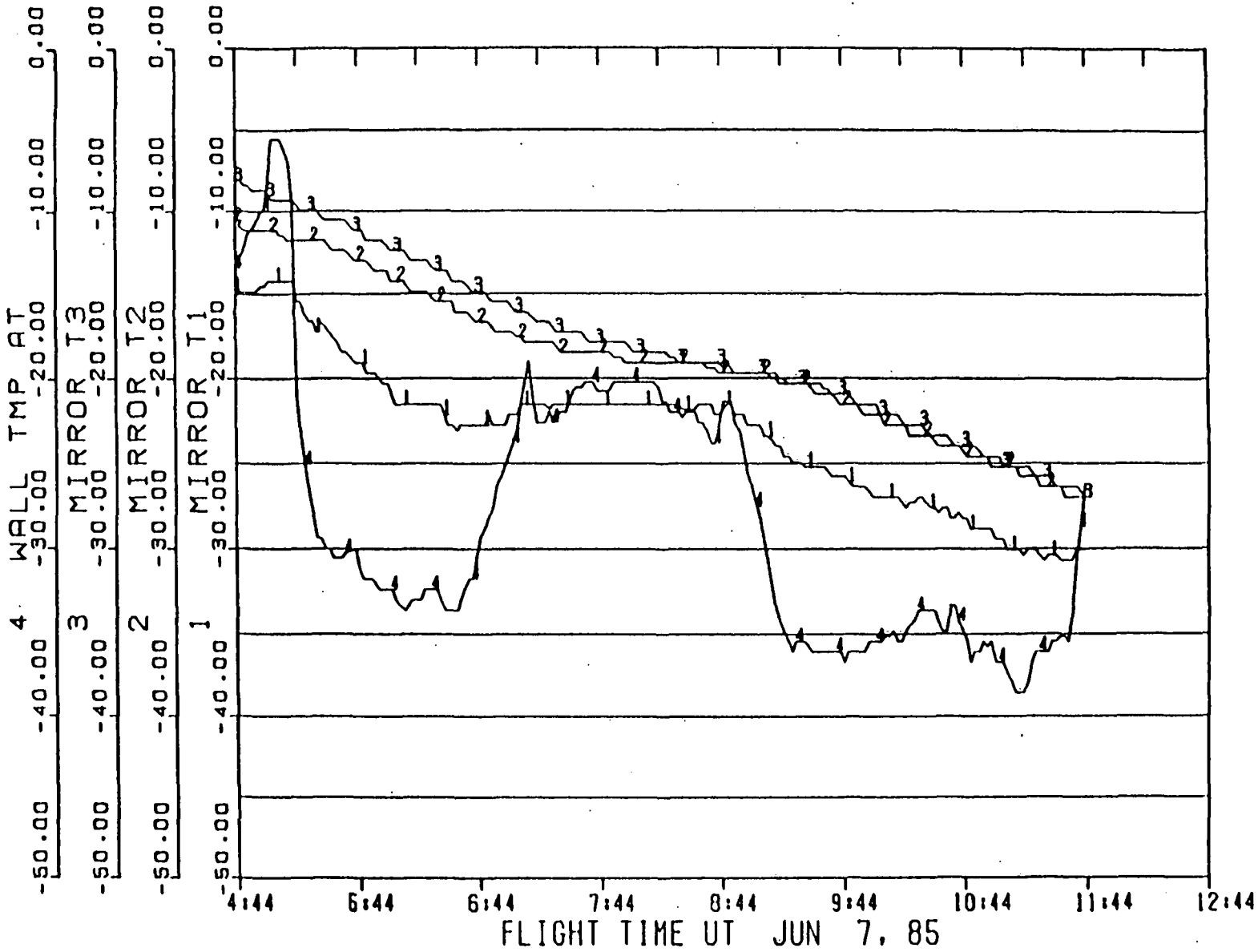

Figure 6. Mean temperature variation with time for KITE Array Flight 2.

a) Mirror temperatures 1, 2, and 3 compared with cavity air temperature.

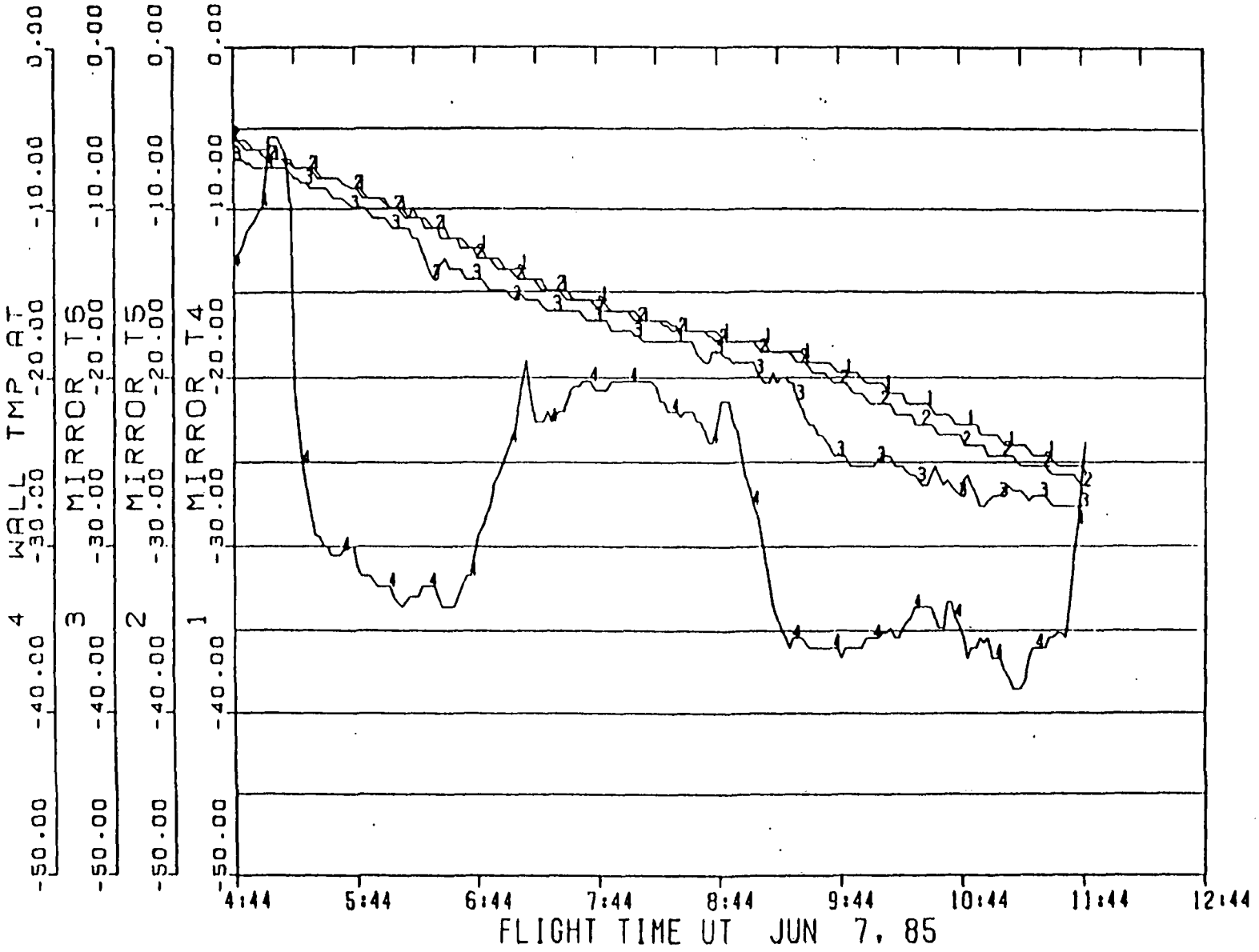

Figure 6. Continued

b) Mirror temperatures 4, 5, and 6 compared with cavity air temperature.

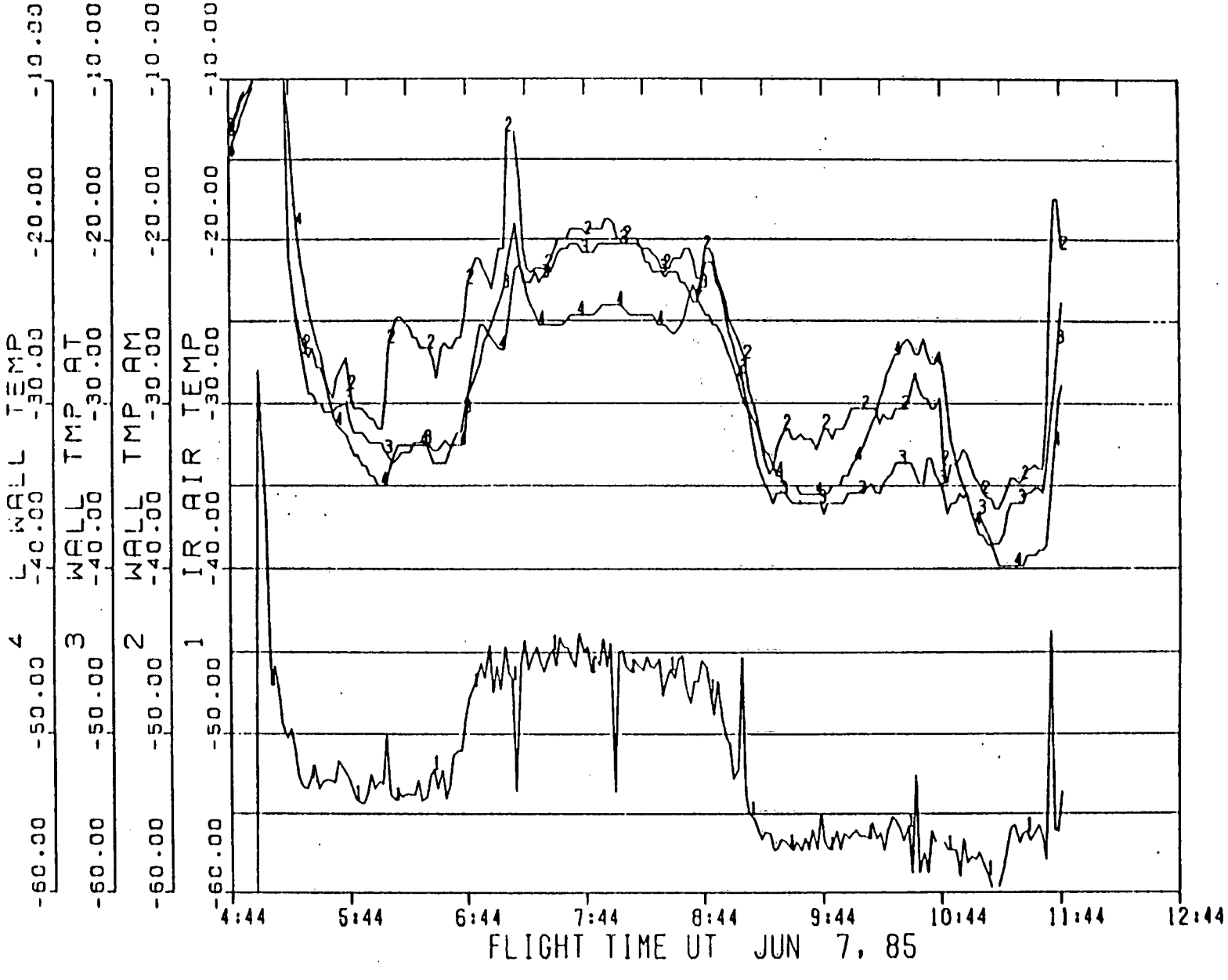

Figure 6. Continued

c) Left wall, IR air and cavity air temperatures.

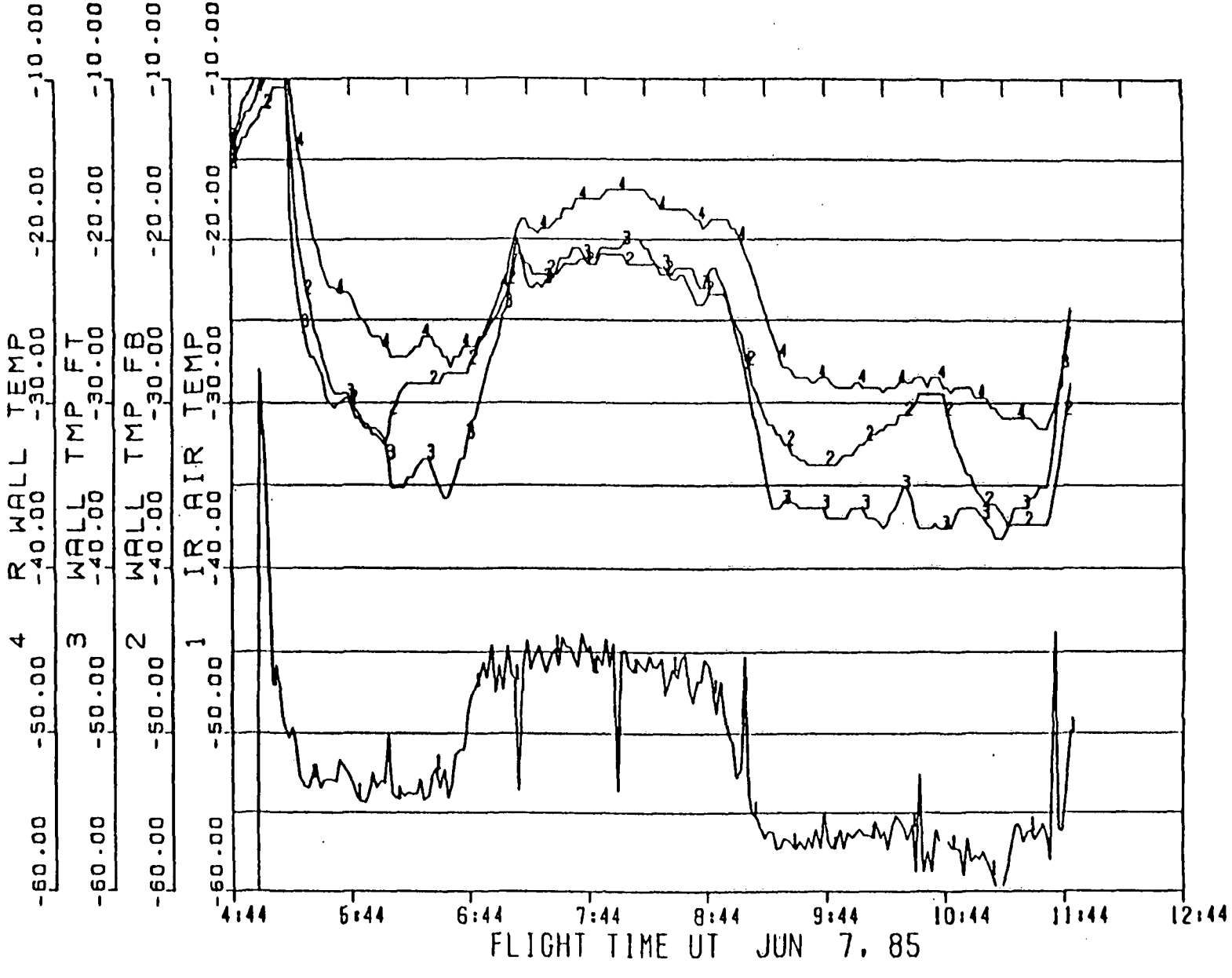

Figure 6. Continued

d) Right wall, IR air and cavity wall temperatures.

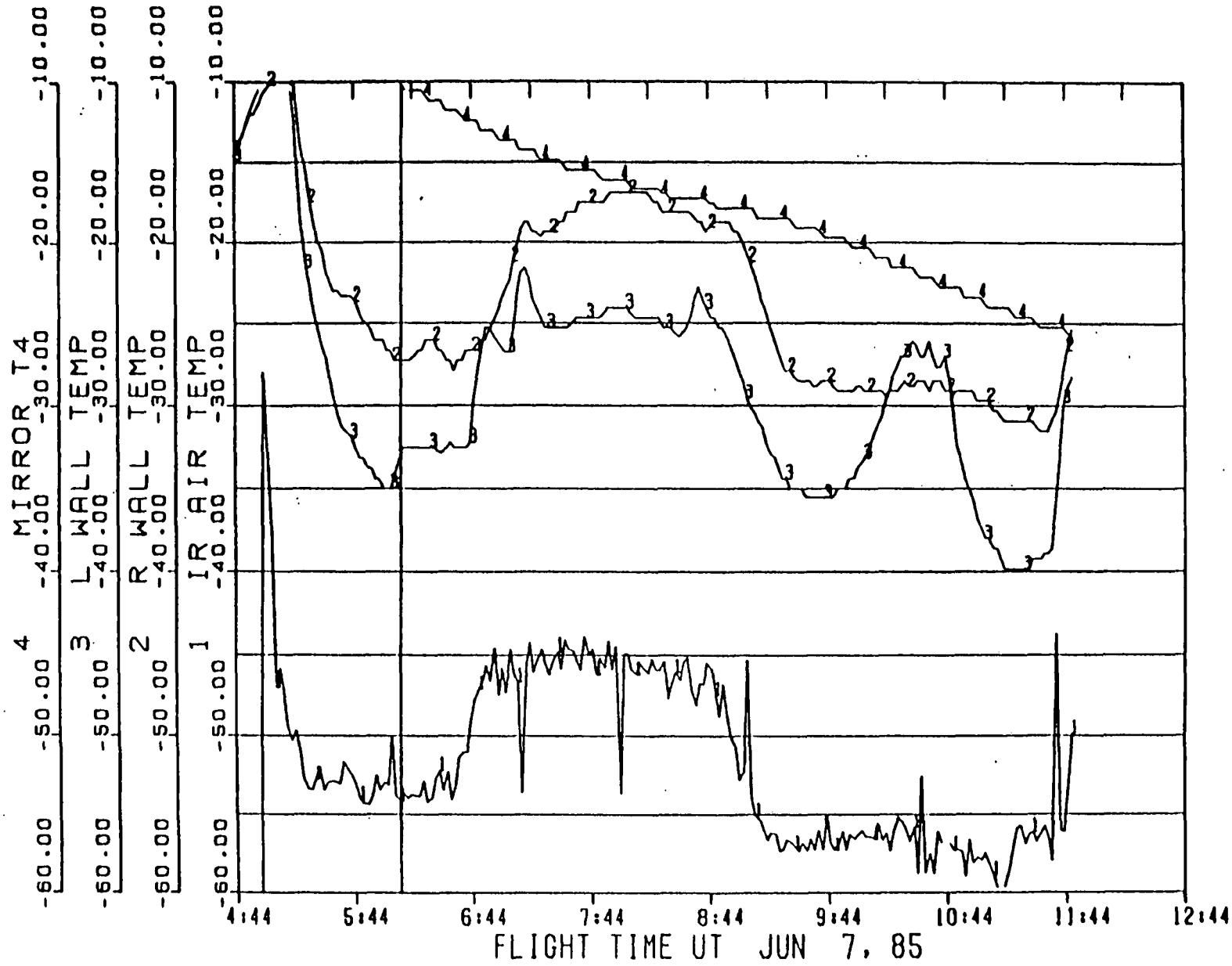

Figure 6. Continued

e) Representative mirror, wall, and IR air temperatures.

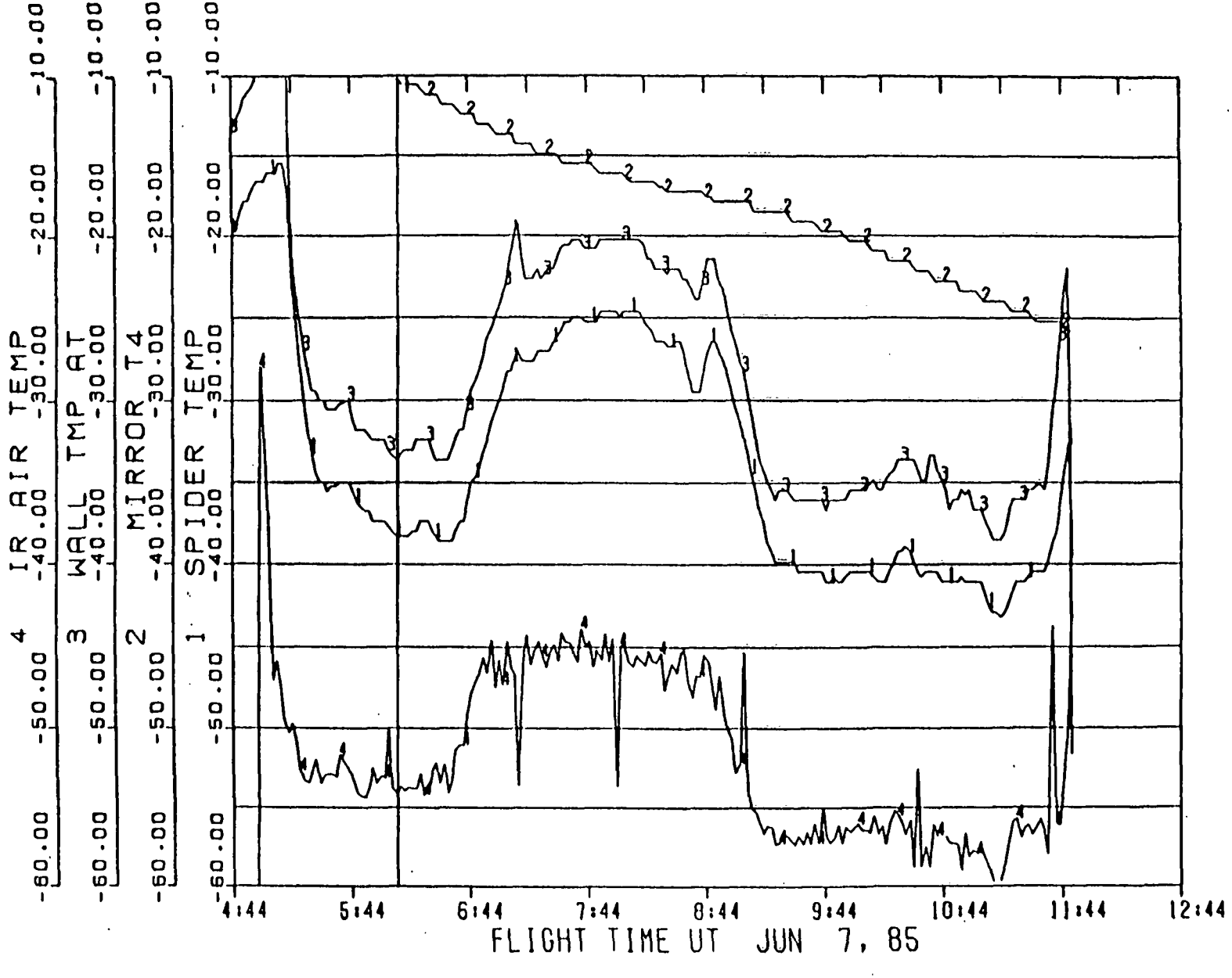

Figure 6. Continued

f) Representative mirror, cavity air, IR air and spider temperatures.

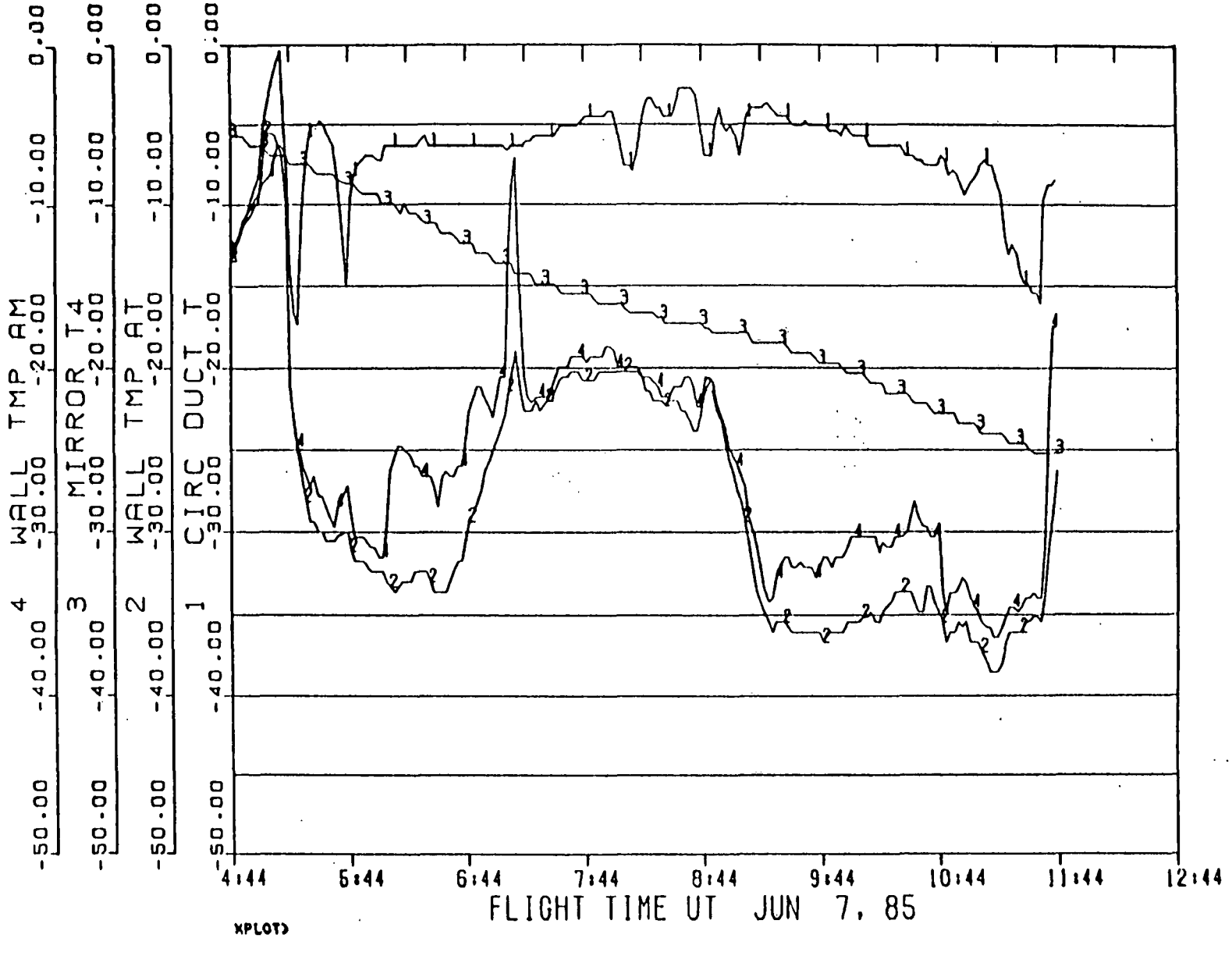

Figure 6. Continued

g) Circulation duct temperatures compared with representative wall mirror and cavity air temperatures.

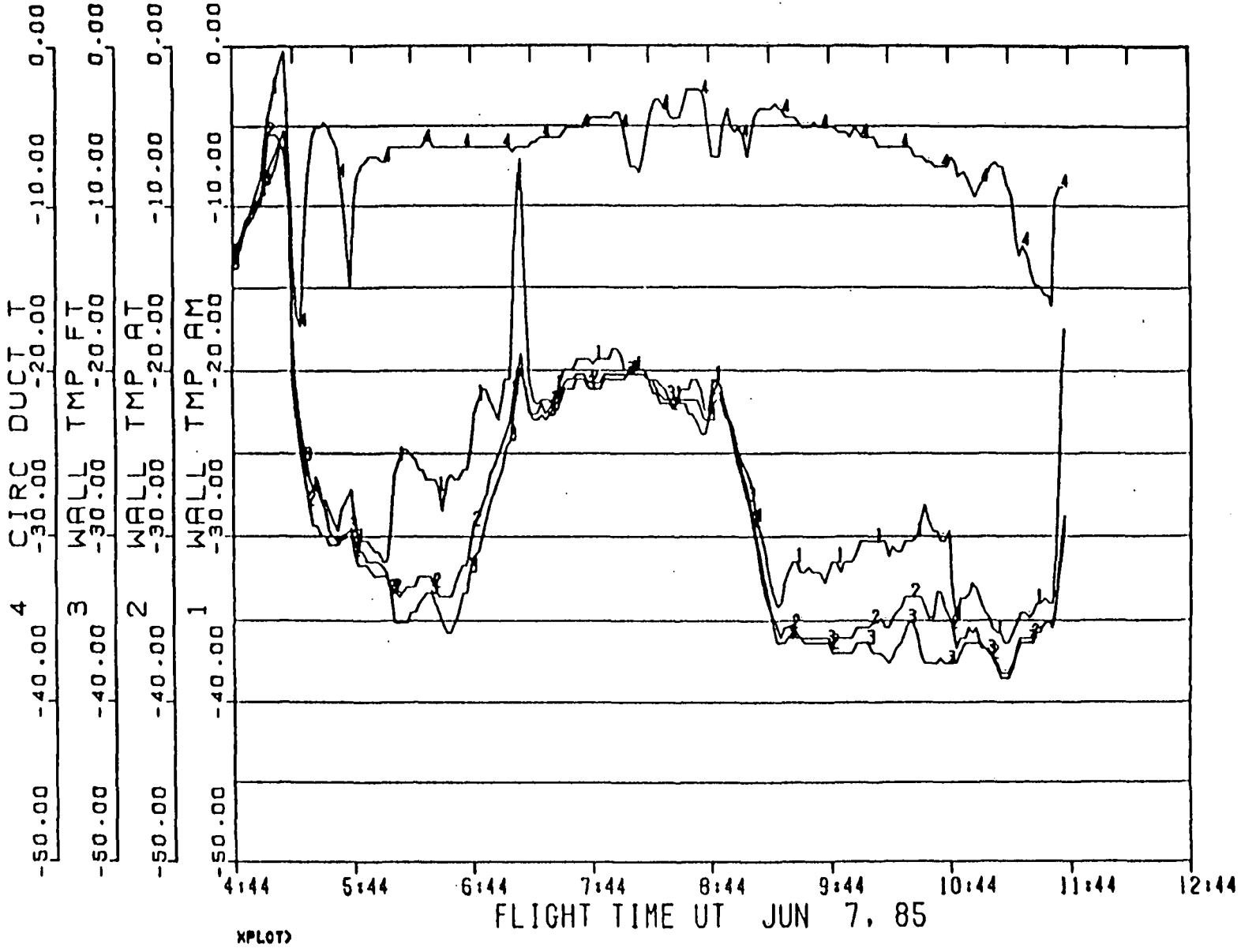

Figure 6. Concluded

h) Circulation duct temperatures compared with representative wall temperatures.

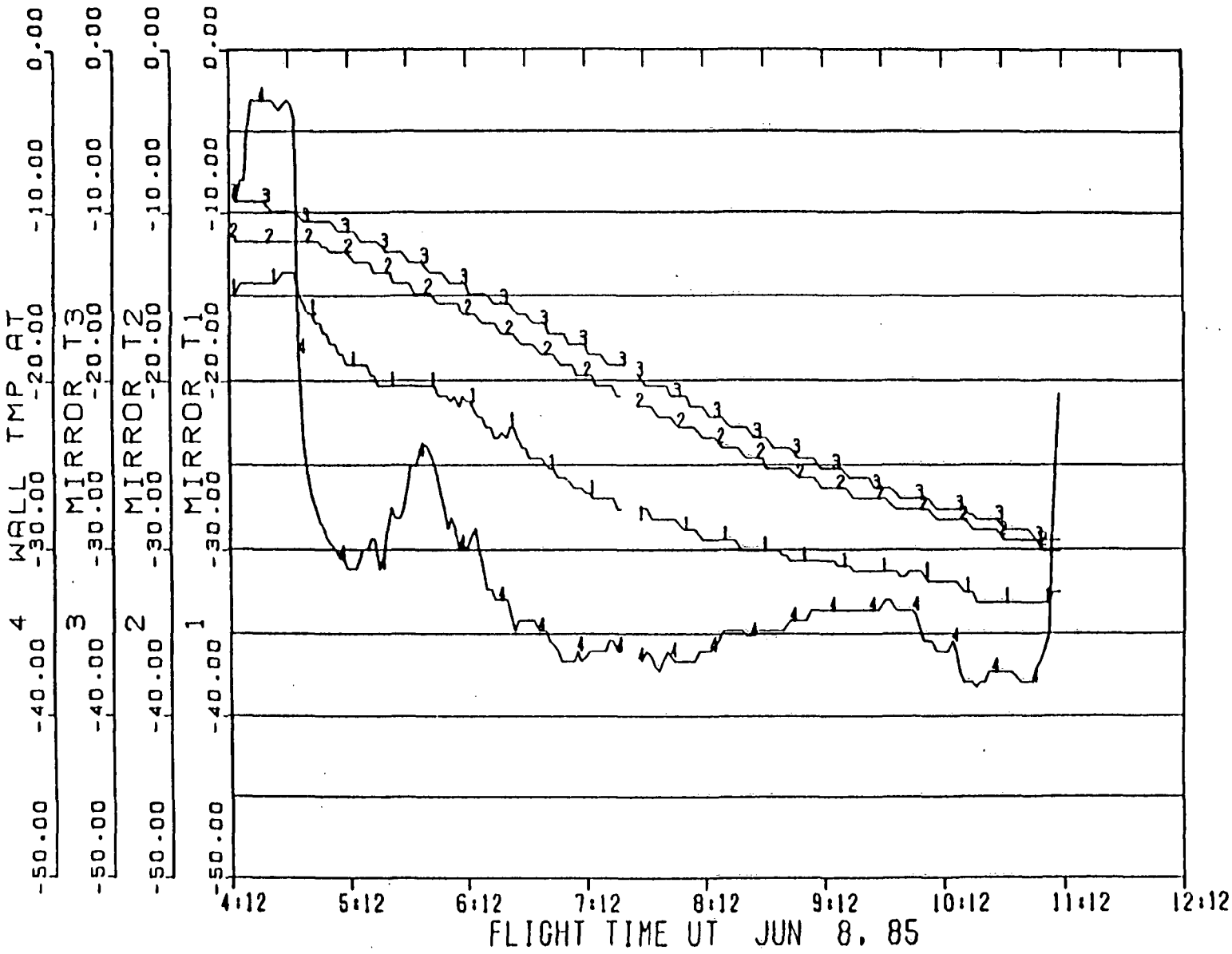

Figure 7. Mean temperature variation with time for KITE Array Flight 3.

a) Mirror temperatures 1, 2 and 3 compared with cavity air temperature.

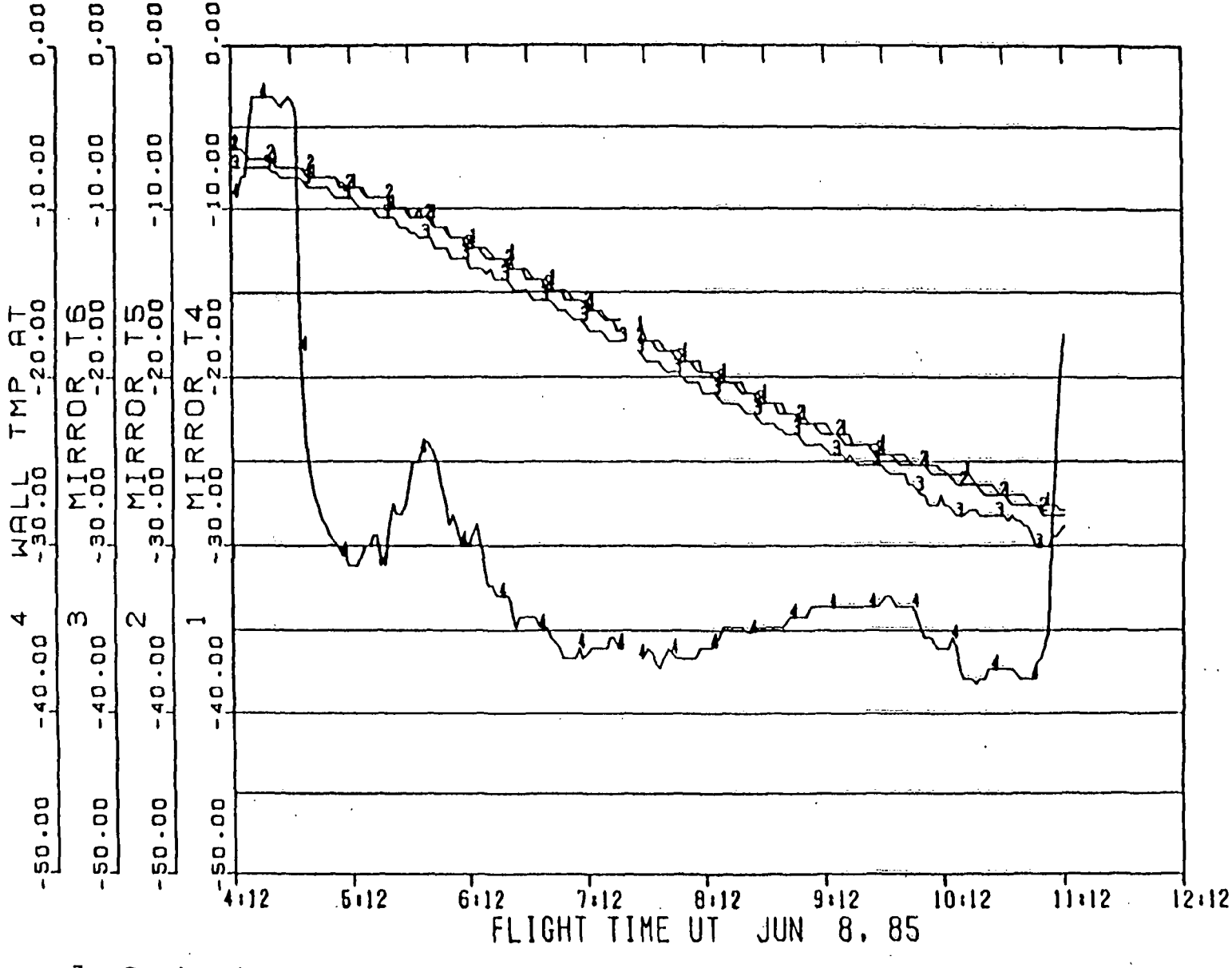

Figure 7. Continued

b) Mirror temperatures 4, 5, and 6 compared with cavity air temperature.

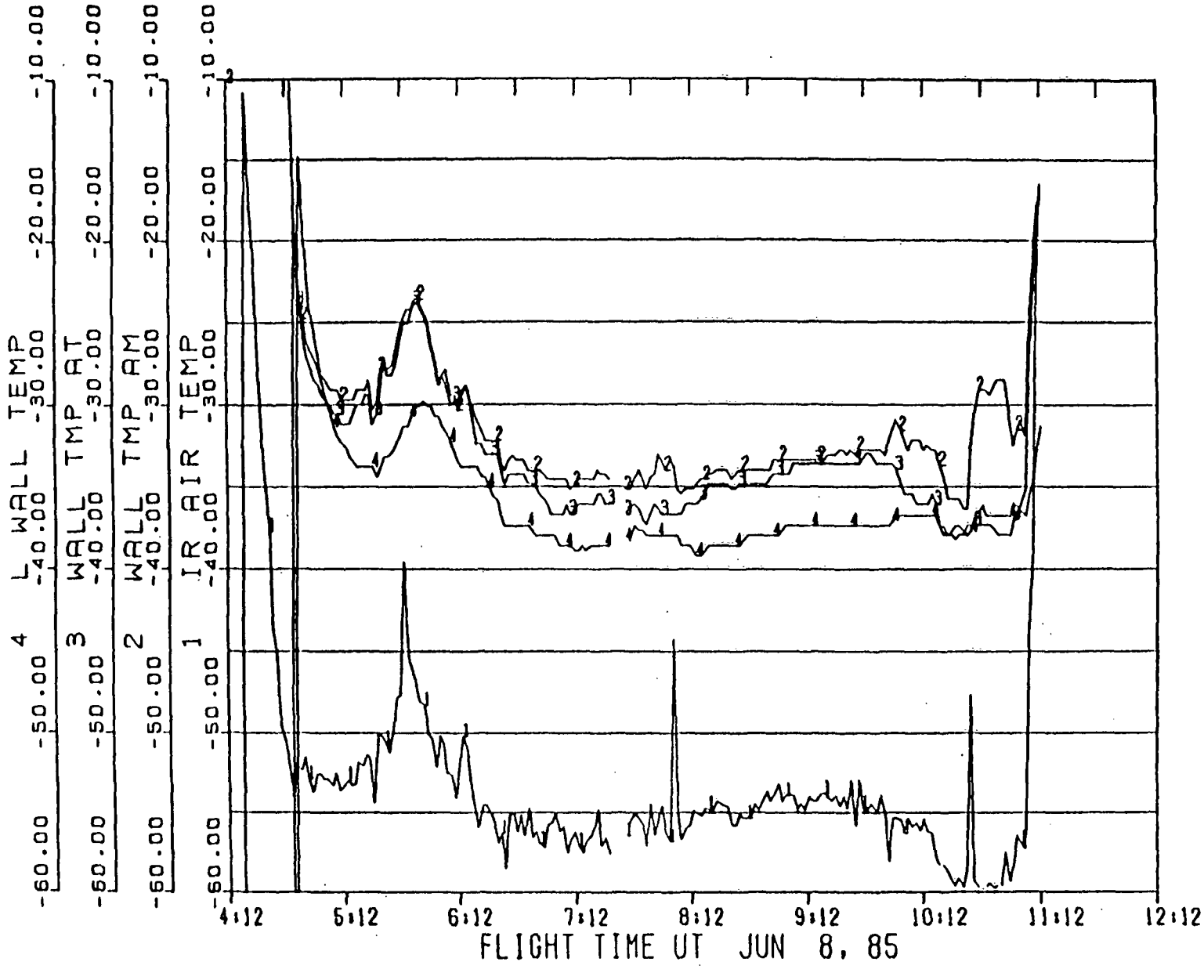

Figure 7. Continued

c) Left wall, IR air and cavity air temperatures.

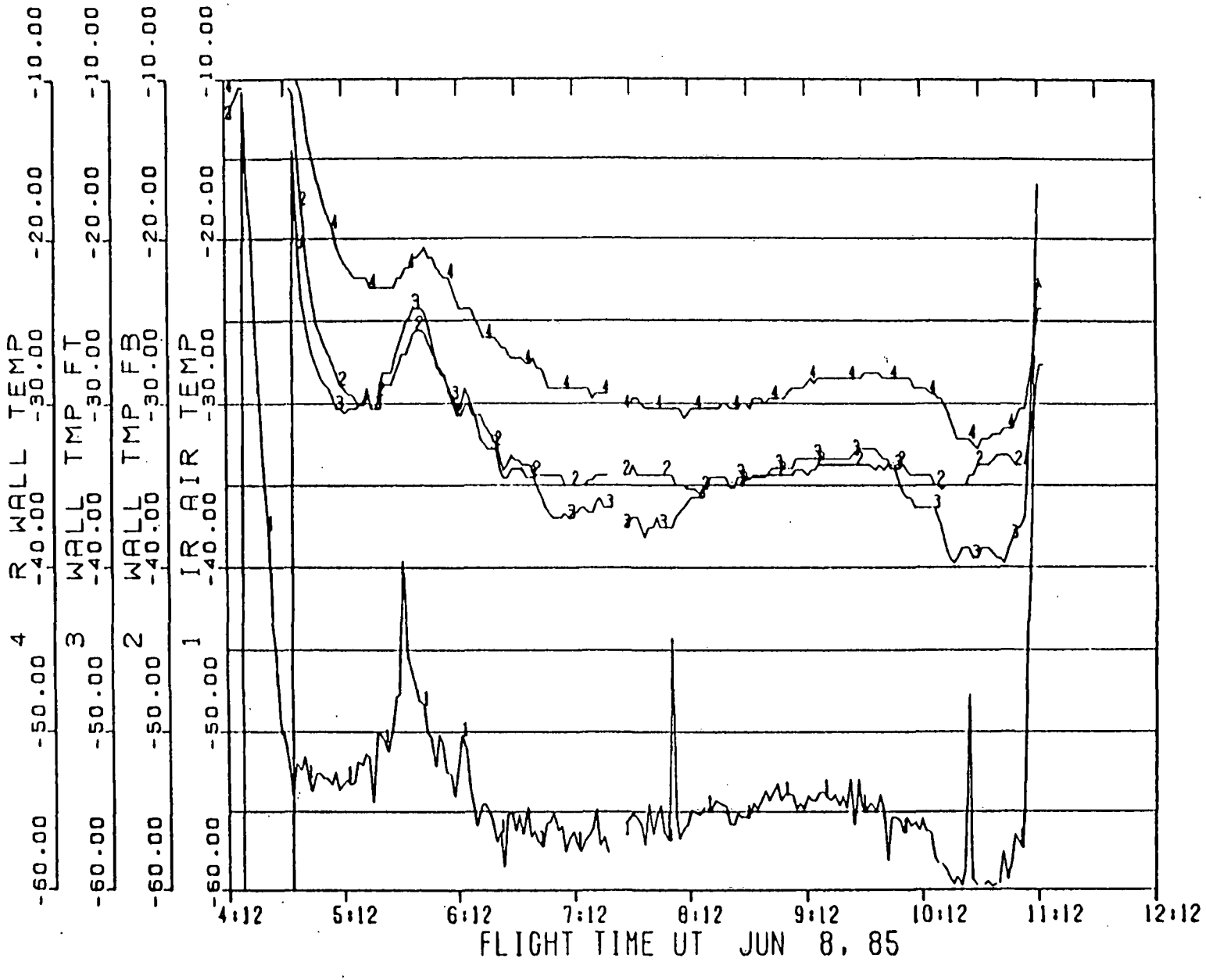

Figure 7. Continued

d) Right wall, IR air and cavity wall temperatures.

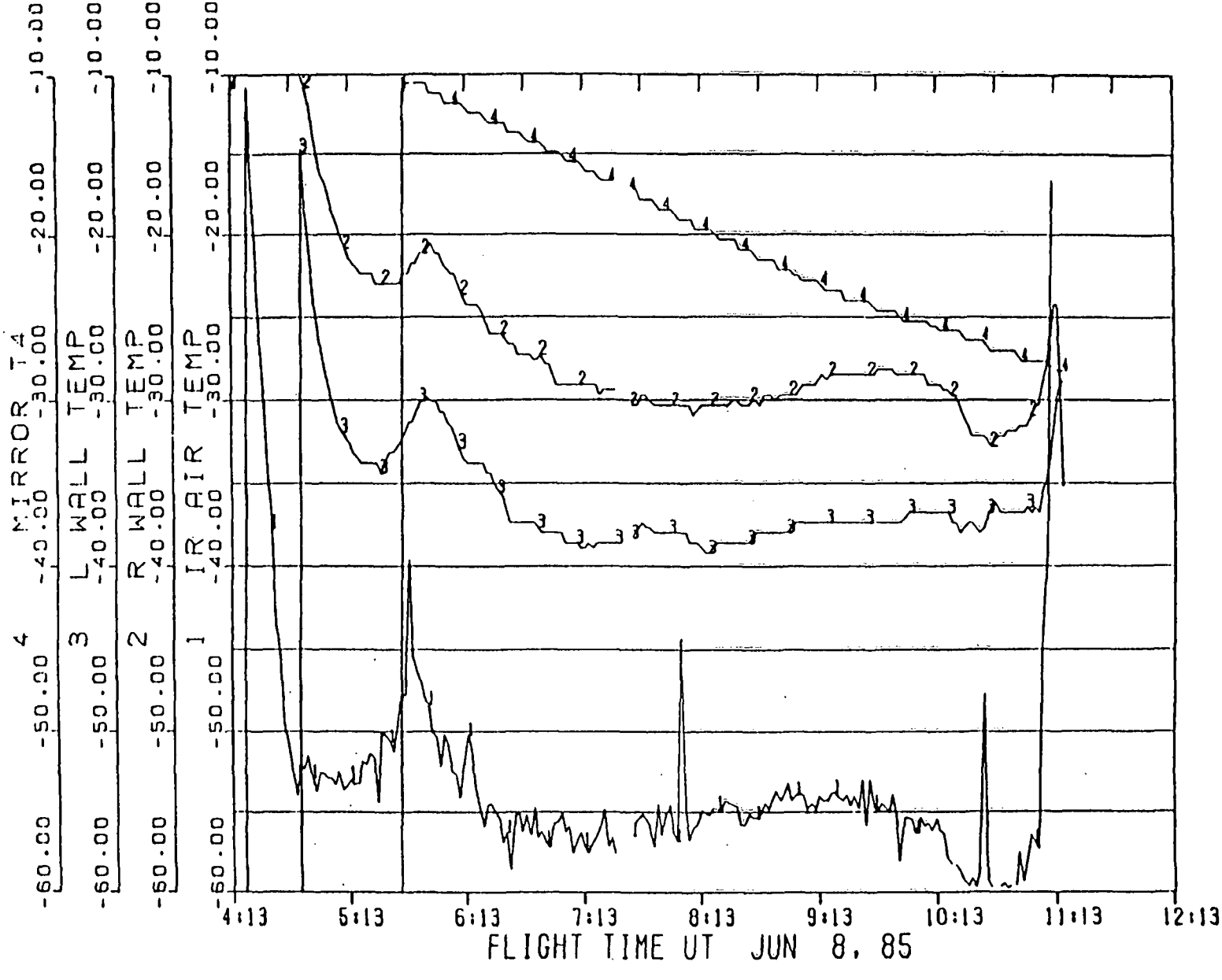

Figure 7. Continued

e) Representative mirror, wall, and IR air temperatures.

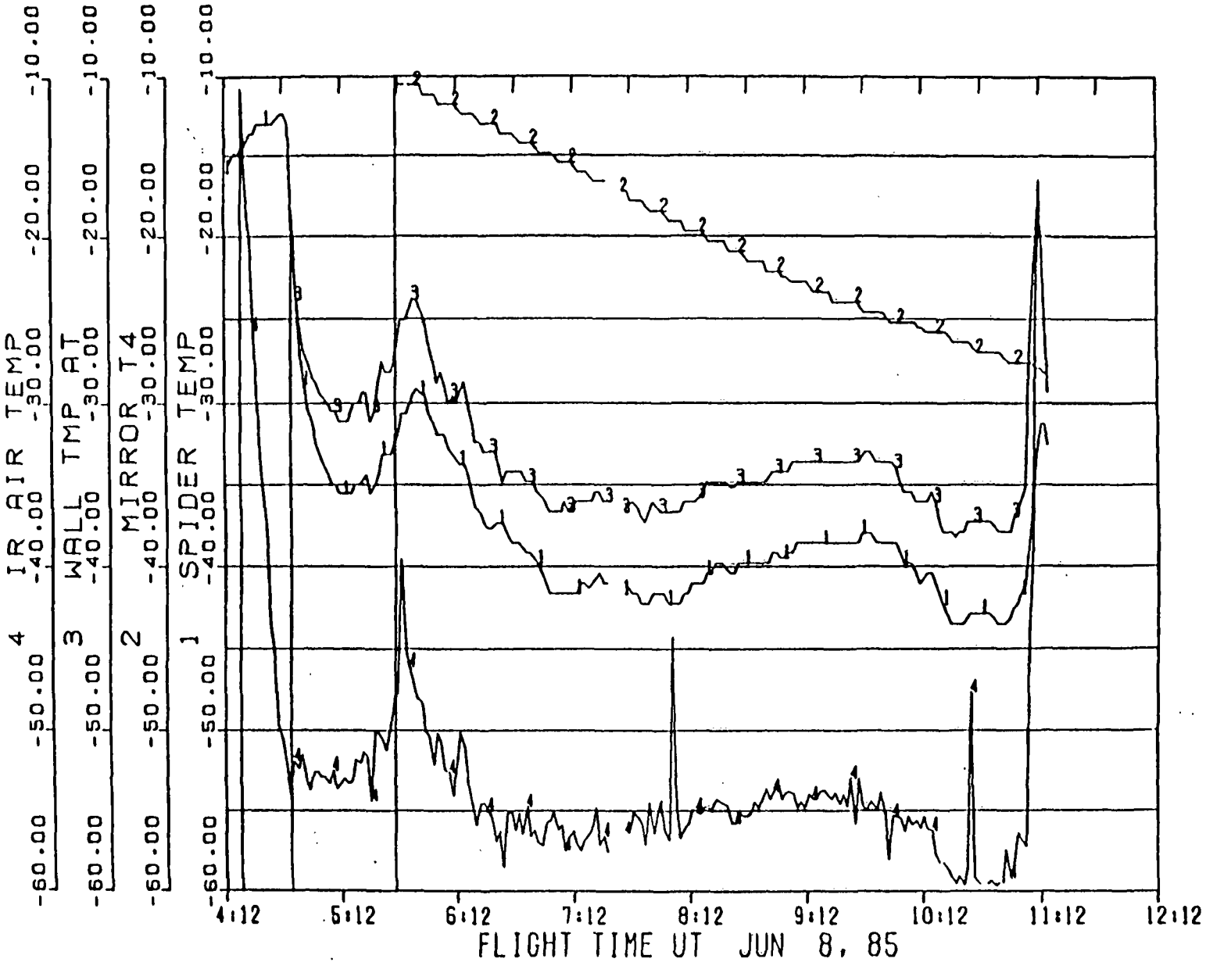

Figure 7. Continued

f) Representative mirror, cavity air, IR air and spider temperatures.

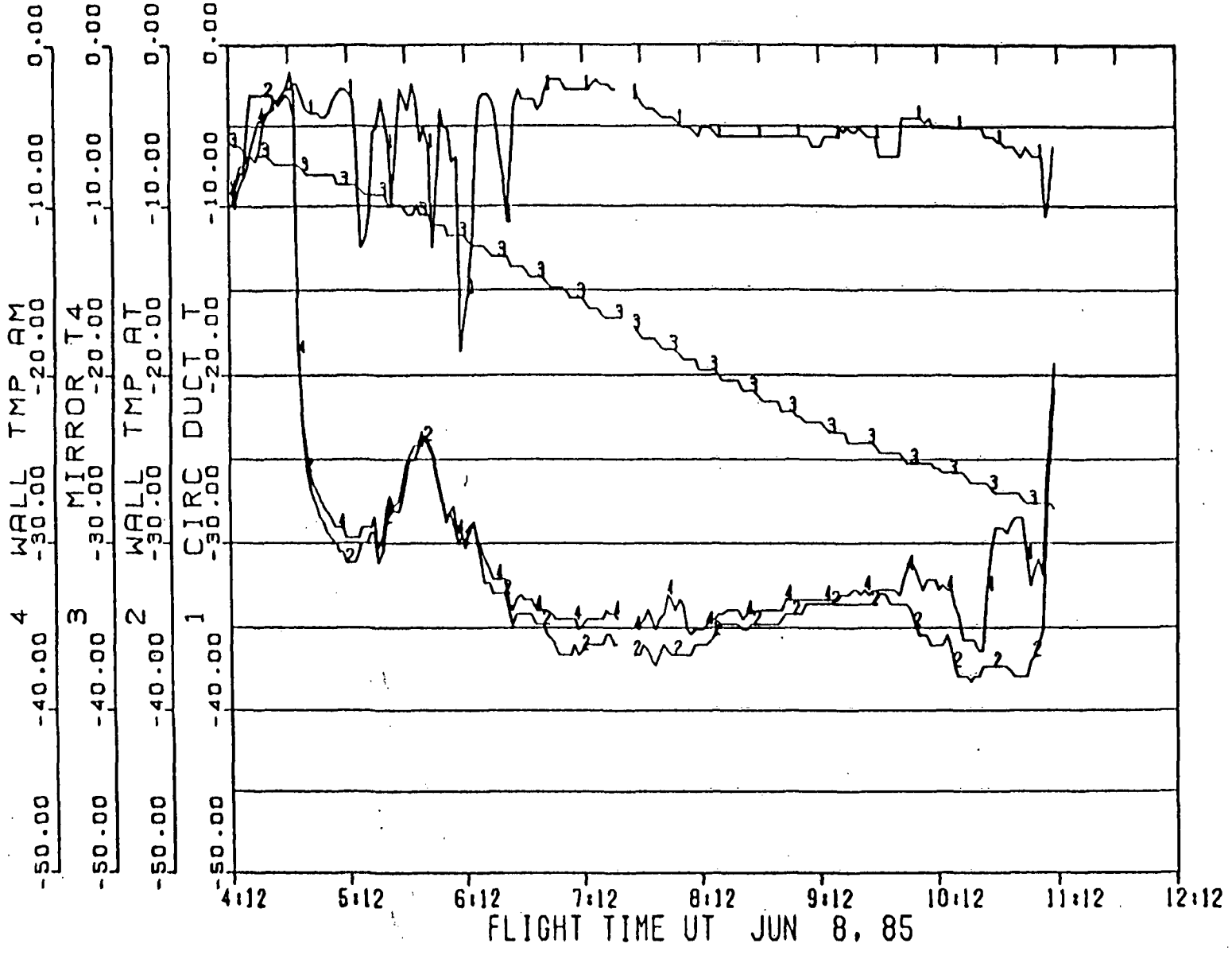

Figure 7. Continued

g) Circulation duct temperatures compared with representative wall mirror and cavity air temperatures.

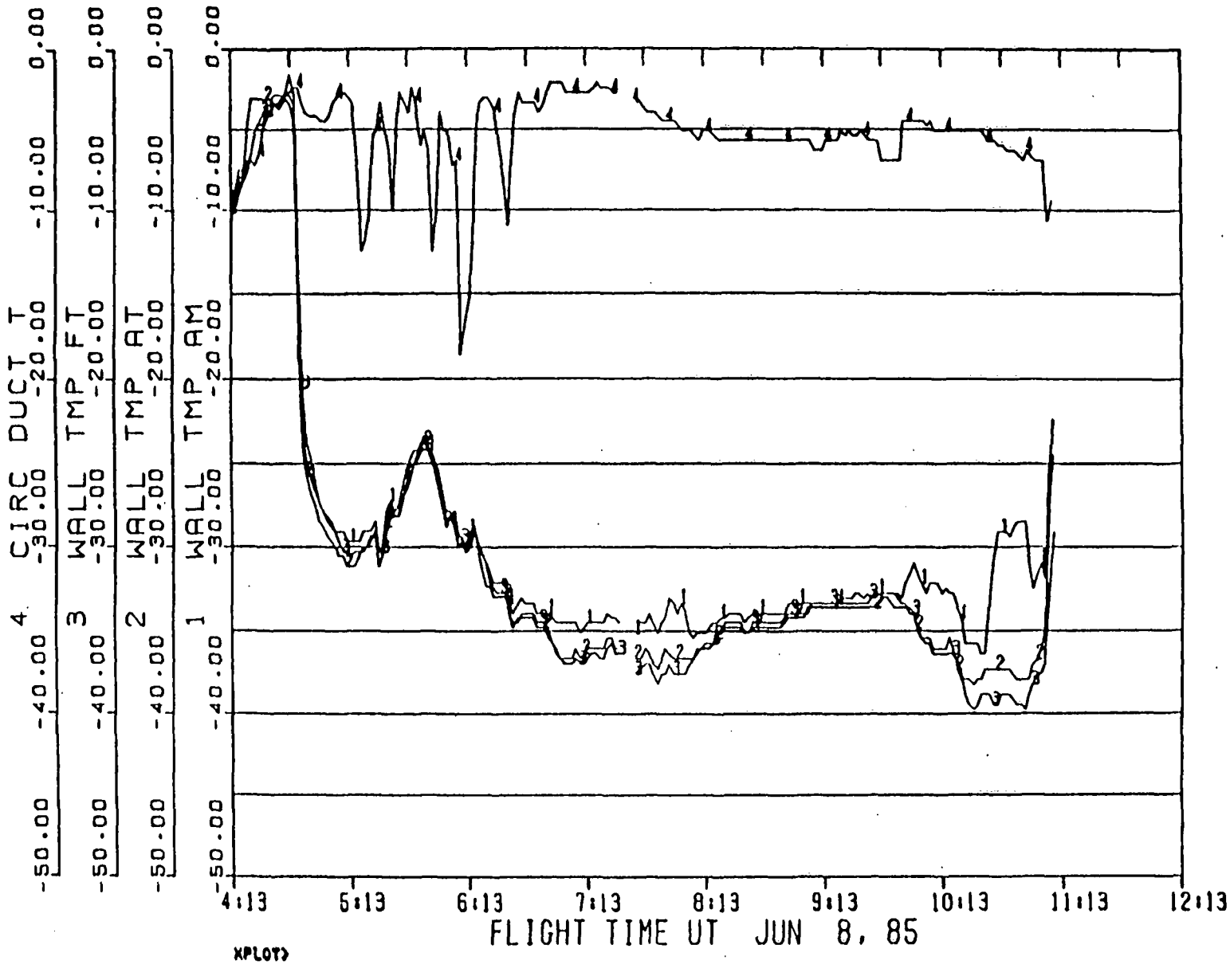

Figure 7. Concluded

h) Circulation duct temperatures compared with representative wall temperatures.